NEDD4L mediates intestinal epithelial cell ferroptosis to restrict inflammatory bowel diseases and colorectal tumorigenesis

Jingjing Liang[1#], Ning Wang[1#], Yihan Yao[1#], Yingmei Wang [2], Xiang An[1], Haofei Wang[1], Huan Liu[3], Yu Jiang[4], Hui Li[5], Xiaoqing Cheng[6], Jiaqi Xu[6], Xiaojing Liang[7], Jun Lou[7], Zengfeng Xin[1], Ting Zhang[8*], Xiaojian Wang[1*], Wenlong Lin[1*]

[1]The Second Affiliated Hospital, Zhejiang University School of Medicine, Hangzhou, China; School of Medicine, Hangzhou City University, Hangzhou, China

[2]State Key Laboratory of Cancer Biology, Department of Pathology, Xijing Hospital and School of Basic Medicine, the Fourth Military Medical University, Xi'an, China

[3]Institute of Basic and Translational Medicine, Xi'an Medical University, Xi'an, China,

[4]Department of Clinical Laboratory Medicine, Second Affiliated Hospital, School of Medicine, Zhejiang University, Hangzhou, China.

[5]Department of Medical Oncology, the Cancer Hospital of the University of Chinese Academy of Sciences (Zhejiang Cancer Hospital)；

[6]Department of Pathology，Sir Run Run Shaw Hospital, Zhejiang University School of Medicine, Hangzhou, China.

[7]Department of Respiratory and Critical Medicine, Sir Run Run Shaw Hospital, Zhejiang University, School of Medicine, Hangzhou, China

[8]Department of Radiation Oncology, The Second Affiliated Hospital, Zhejiang University School of Medicine, Hangzhou, China

[#]These authors contributed equally.

[*]Address correspondence to: Wenlong Lin, Zhejiang University, 866 Yuhang Tang Road, Hangzhou, Zhejiang, P. R. China. Phone: 86.0571.88981662; Email: lwl210@foxmail.com. Or to: Xiaojian Wang, Zhejiang University, 866 Yuhang Tang Road, Hangzhou, Zhejiang, P. R. China; Phone: 86.0571.88201220; Email: wangxiaojian@cad.zju.edu.cn. Or to: Ting Zhang, The Second Affiliated Hospital, Zhejiang University School of Medicine, Zhejiang, P. R. China; Phone: 86.0571. 87783521; Email: zezht@zju.edu.cn.

Abstract

Various factors play key roles in maintaining intestine homeostasis. Disruption of the balance may lead to intestinal inflammatory diseases (IBDs) and even colorectal cancer (CRC). Loss or gain of function of many key proteins can result in dysregulated intestinal homeostasis. Our research demonstrated that neural precursor cells expressed developmentally down-regulated 4-like protein (NEDD4L or NEDD4-2), a type of HECT family E3 ubiquitin ligase, played an important role in maintaining intestinal homeostasis. NEDD4L expression was significantly inhibited in intestinal epithelial cells (IECs) of patients with Crohn's disease (CD), ulcerative colitis (UC), and CRC. Global knockout of NEDD4L or its deficiency in IECs exacerbated dextran sulfate sodium (DSS)-/2,4,6-trinitrobenzene sulfonic acid (TNBS)-induced colitis and azoxymethane (AOM)/DSS-induced colorectal cancer. Mechanistically, NEDD4L deficiency in IECs inhibited the key ferroptosis regulator glutathione peroxidase 4 (GPX4) expression by reducing the protein expression of solute carrier family 3 member 2 (SLC3A2) without affecting its gene expression, ultimately promoting DSS-induced IEC ferroptosis. Importantly, ferroptosis inhibitors reduced the susceptibility of NEDD4L-deficient mice to colitis and colitis-associated colorectal cancer (CAC). Thus, NEDD4L is an important regulator in IEC ferroptosis, maintaining intestinal homeostasis, making it a potential clinical target for diagnosing and treating IBDs.

Introduction

The intestinal mucosa is the largest mucosal surface that communicates with the environment, dietary antigens, and various microorganisms, serving as a critical component of immune regulation(1, 2). The intestinal mucosal barrier, composed of the intestinal epithelial cells (IECs), the immune barrier, and the intestinal flora barrier (3), jointly maintains intestinal homeostasis. Intestinal disorders caused by various factors such as diet, genetic susceptibility, environmental factors, and mucosal immune disorders contribute to the development of intestinal diseases, including colitis and colorectal cancer (CRC)(4). Therefore, maintaining intestinal mucosa homeostasis is crucial for controlling inflammation and preventing excessive immunopathology following inflammation.

Inflammatory bowel diseases (IBDs), including Crohn's disease (CD) and ulcerative colitis (UC), are complicated diseases characterized by abnormal mucosal immune responses triggered by microorganisms, cytokines, and damaged epithelial cells, which can exacerbate the inflammation during the pathogenesis of colitis(4). Ferroptosis, a kind of cell death induced by excessive ferric ion levels and lipid peroxidation, exhibits a distinct morphology from other forms of cell death, such as apoptosis, necroptosis, and pyroptosis. Playing a crucial role in a variety of tissues and cell types, including neuron cells, renal tubular epithelial cells, endothelial cells, and T cells (5, 6), ferroptosis regulates diseases associated with cell death. Proteins like glutathione peroxidase 4 (GPX4), solute carrier family 7 member 3 (SLC7A11), solute carrier family 3 member 2 (SLC3A2), and others directly or indirectly participate in the regulation of ferroptosis (5, 7). The ferroptosis of many tumor cells can be modulated by adjusting the expression levels of GPX4, SLC7A11,

and intracellular lipid peroxidation (8). However, only a few studies have reported on ferroptosis in intestine homeostasis (9, 10), and the regulatory function of SLC3A2 in ferroptosis remains largely unclear (11).

Numerous key proteins play important roles in maintaining the homeostasis of IECs (12, 13). E3 ubiquitin ligases, such as TNF alpha induced protein 3 (TNFAIP3, A20), baculoviral IAP repeat containing 2 (BIRC2, cIAP1), baculoviral IAP repeat containing 3 (BIRC3, cIAP2), tripartite motif containing 31 (TRIM31), ring finger protein 186 (RNF186) , and membrane associated ring-CH-type finger 3 (MARCH3), serve as key negative regulators in multiple signal pathways, participating in intestinal homeostasis by regulating immune response, intestinal epithelial cell proliferation, apoptosis, or necroptosis(14-20). Neural precursor cells expressed developmentally down-regulated 4-like protein (NEDD4L), a member of the E3 ubiquitin ligase HECT family, is essential for maintaining cell homeostasis as it can bind and regulate a variety of membrane proteins (21). NEDD4L has an amino-terminal Ca^{2+} phospholipid binding (C2) domain, a protein-protein interaction (WW) domain, and a HECT domain located at the carboxyl-terminal (22). The most clearly studied target of NEDD4L is the epithelial sodium channel (ENaC), which is usually expressed in lung and kidney epithelial cells, participating in related diseases (23-25). It also mediates the polyubiquitination and degradation of Smad2/3, thereby limiting the TGF-β signaling pathway (26). However, the regulatory role of NEDD4L in IBDs and colitis-associated colorectal cancer (CAC) remains unclear (27).

Here, we identified that both the gene and protein expression of NEDD4L were significantly inhibited in the IECs of patients with colitis and CRC, and negatively correlated

with the disease status of colitis. NEDD4L deficiency in mice promoted dextran sulfate sodium (DSS)-/2,4,6-trinitrobenzene sulfonic acid (TNBS)-induced colitis and azoxymethane (AOM)/DSS-induced colorectal cancer. Mechanistically, NEDD4L deficiency in IECs reduced the protein expression of the soluble amino acid transport protein SLC3A2 without affecting its gene expression. This led to the inhibition of the key ferroptosis regulator GPX4 expression, ultimately promoting DSS-induced IEC ferroptosis. Importantly, ferroptosis inhibitors, such as ferrostatin-1 (Fer-1) and deferoxamine mesylate (DFOM), reversed the colitis and CAC phenotype difference between wild-type (WT) and NEDD4L IEC-deficient (*Nedd4l*$^{f/f}$ *Villin*^{Cre}) mice. Collectively, our data demonstrated that NEDD4L acted as an important regulator in IEC ferroptosis, thus maintaining intestinal homeostasis and controlling the development of colitis and CAC, suggesting that NEDD4L might be a potential target for the diagnosis and treatment of these diseases.

Results

NEDD4L expression is inhibited in IBDs

Our previous data have demonstrated that NEDD4L plays a crucial role in IL-17-, IL-6-, and viruses-mediated innate immune responses (28-30). However, its role in intestinal homeostasis remains unclear. To explore the potential function of NEDD4L in intestinal homeostasis, we first analyzed the *NEDD4L* gene expression in the public database. As shown in Supplementary Figure 1, A and B, the *NEDD4L* gene was highly expressed in human neuron, lung, and intestinal systems, particularly highest in goblet cells, but was lowly expressed in the human immune system, indicating that highly expressed *NEDD4L* in intestinal epithelium might be involved in maintaining intestinal homeostasis. We analyzed the gene expression of *NEDD4L* in patients with IBDs from GEO datasets. As shown in Supplementary Figure 1, C-E, compared to the healthy control (HC), *NEDD4L* gene expression in colonic mucosa was restricted in patients with CD and UC. Nevertheless, *NEDD4L* gene expression was significantly increased in PBMCs from patients with CD and UC compared with HC (Supplementary Figure 1F). Two cohorts of study subjects from the Xijing Hospital (cohort1) and First Affiliated Hospital of Zhejiang University, School of Medicine (FAHZU, cohort2) were recruited to trace the NEDD4L protein expression in the colonic biopsies. As shown in Figure 1, A-D, the NEDD4L protein level in IECs was significantly reduced in patients with UC and CD compared to the normal control subjects (HC). In the samples from cohort1, only 4.8% of the biopsies from patients with UC (4/83) exhibited strong NEDD4L immunohistochemistry (IHC) staining, whereas 20% of the healthy control subjects (8/40) showed strong NEDD4L IHC staining ($p<0.001$;

table 1). Similar results were observed in cohort2, only 38.8% of the UC patient biopsies (14/36) and 39.0% of the CD patient biopsies (16/41) exhibited strong NEDD4L IHC staining, whereas 96.8% of the healthy control subjects (30/31) showed strong NEDD4L IHC staining ($p<0.001$; table 2). Importantly, NEDD4L protein expression was lower in patients with moderate or severe colitis than in those with mild colitis from cohort2 (Figure 1, E and F), consistent with the GEO data (Supplementary Figure 1G), indicating that NEDD4L expression was negatively correlated with the severity of colitis. Similarly, *NEDD4L* gene expression in colonic mucosa was significantly inhibited in the diseased individual from monozygotic twin pairs discordant for ulcerative colitis compared to the healthy individual (Supplementary Figure 1H), suggesting that the reduced expression of *NEDD4L* was likely to be a consequence of IEC damage or inflammation. To further explore the specific expression profile of *NEDD4L* in IECs, a single-cell RNA analysis was performed. Compared to the healthy tissue, the gene expression of *NEDD4L* in inflamed colon tissues from patients with UC was significantly inhibited in enterocytes (including bestrophin 4 (Best4)$^+$ enterocytes, immature enterocytes2), goblet, transit-amplifying cell (TA, including TA1, TA2, cycling TA, and secretory TA), stem cells, but not significantly changed in enterocytes progenitors, enteroendocrine, immature enterocyets1, M cells, and tuft cells (Supplementary Figure 1I). Furthermore, both the gene and protein expression of NEDD4L in patients with IBDs were significantly inhibited compared to the normal colon mucosa (Figure 1, G and H). Additionally, upon DSS treatment in mice, both the gene and protein expression of NEDD4L in IECs were significantly inhibited (Figure 1, I and J and Supplementary Figure 1, J and K). Collectively, these results suggest that the NEDD4L

gene and protein were significantly inhibited in humans and mice with colitis, and NEDD4L expression was correlated with the severity of patients with IBDs.

Nedd4l deficiency in mice enhances sensitivity to experimental colitis

To investigate the role of NEDD4L in colitis, *Nedd4l* heterogeneous knockout mice (*Nedd4l*$^{+/-}$) and control wild-type littermates (*Nedd4l*$^{+/+}$) were initially challenged with 4% DSS to induce an acute experimental colitis model. The mortality rate was significantly higher in *Nedd4l*$^{+/-}$ mice compared to *Nedd4l*$^{+/+}$ mice (Figure 2A). Remarkably, we observed more severe colitis after 3% DSS treatment in *Nedd4l*$^{+/-}$ mice compared to *Nedd4l*$^{+/+}$ mice, as evidenced by significantly greater body weight loss, higher rectal bleeding score, and shorter colons in DSS-treated *Nedd4l*$^{+/-}$ mice (Figure 2, B-F). Furthermore, *Nedd4l* global deficient mice (*Nedd4l*$^{-/-}$, KO) exhibited a more severe colitis phenotype when treated with a very low dosage of DSS (1%), which was hard to induce obvious colitis phenotype in *Nedd4l*$^{+/-}$ and *Nedd4l*$^{+/+}$ mice, suggesting that *Nedd4l* knockout increased the susceptibility of mice to low-dose DSS exposure (Supplementary Figure 2, A-E).

To determine whether *Nedd4l* deficiency in IECs or hematopoietic cells contributes to the more severe colitis phenotype, bone marrow chimera experiments were conducted. Lethally irradiated *Nedd4l*$^{+/+}$(WT) and *Nedd4l*$^{-/-}$(KO) mice were reconstituted with bone marrow cells from WT mice. Mice reconstituted with *Nedd4l* deficiency in non-hematopoietic cells (WT→KO) exhibited a more severe colitis phenotype compared to the *Nedd4l*$^{+/+}$ chimeras (WT→WT) following DSS treatment (Figure 2, G-J). Collectively, these data implicate that NEDD4L in non-hematopoietic cells promoted the pathogenesis of DSS-

induced colitis.

Nedd4l deficiency in IECs exacerbates DSS-induced and TNBS-induced experimental colitis

To further explore whether the protective role of NEDD4L in colitis was intrinsic to IECs, we generated IEC-specific *Nedd4l* knockout mice (*Nedd4l*$^{f/f}$ *Villin*^{Cre}) by crossing *Nedd4l* floxed mice (*Nedd4l*$^{f/f}$) with *Villin*^{Cre} mice, resulting in constitutive deletion of *Nedd4l* in the IECs. Consistent with previous reports (31), *Nedd4l*$^{f/f}$ *Villin*^{Cre} mice displayed normal intestinal histology. The terminally differentiated cells were indistinguishable between wild-type and *Nedd4l*$^{f/f}$ *Villin*^{Cre} mice under steady-state conditions (Supplementary Figure 2, F and G). In addition, assessment of the numbers of goblet cells, Paneth cells, enteroendocrine, and enterocytes (identified by periodic acid–Schiff (PAS), lysozyme (Lyz), chromogranin A (ChgA), and alkaline phosphatase (ALP) staining, respectively) revealed no obvious difference in terms of cell lineage commitment (Supplementary Figure 2, F-I). This observation was further confirmed by qPCR analysis, which showed no significant alterations in the expression of marker genes for the different cell lineages and stem cell populations in intestinal tissue from *Nedd4l*$^{f/f}$ *Villin*^{Cre} mice compared with control *Nedd4l*$^{f/f}$ mice (Supplementary Figure 2, J and K). However, *Nedd4l*$^{f/f}$ *Villin*^{Cre} mice showed a significantly higher death rate than control littermates upon 2.5% DSS treatment (Figure 3A). *Nedd4l*$^{f/f}$ *Villin*^{Cre} mice exhibited more severe weight loss, rectal bleeding, colon shortening, epithelial damage, and crypt architecture disruption than *Nedd4l*$^{f/f}$ mice when challenged with 2% DSS (Figure 3, B-F). Additionally, a 5-day DSS treatment induced comparable degrees and absolute cell numbers of mucous-infiltrated monocytes,

221 macrophages, and neutrophils, but increased absolute cell numbers of mucous-infiltrated
222 T cells and B cells in *Nedd4l*$^{f/f}$ *Villin*^{Cre} mice compared with the control littermates (Figure
223 3G). Moreover, following the development of colitis, particularly on day 9, much more
224 inflammatory immune cell infiltration in mucous was observed in *Nedd4l*$^{f/f}$ *Villin*^{Cre} mice
225 compared to *Nedd4l*$^{f/f}$ mice, including monocytes, macrophages, T cells, and B cells
226 (Figure 3H).

227 We then investigated whether *Nedd4l* deficiency might exacerbate colitis in an
228 alternative model induced by TNBS. As expected, compared with the control group, TNBS-
229 treated *Nedd4l*$^{f/f}$ *Villin*^{Cre} mice phenocopied the aggravated symptoms of colitis as in DSS-
230 treated *Nedd4l*$^{f/f}$ *Villin*^{Cre} mice (Supplemental Figure 3, A-F). Collectively, these data
231 support the notion that *Nedd4l* deficiency in IECs contributed both to DSS-induced and
232 TNBS-induced colonic damage and colitis.

233 **_Nedd4l_ deficiency in IECs promotes IEC ferroptosis and subsequent intestinal**
234 **barrier integrity damage**

235 To explore the underlying mechanisms of NEDD4L in regulating colitis, colonic tissues from
236 DSS-treated *Nedd4l*$^{f/f}$ *Villin*^{Cre} mice and *Nedd4l*$^{f/f}$ littermates were subjected to RNA-
237 sequencing analysis. As shown in Figure 4A, the tight junction signaling was significantly
238 downregulated in *Nedd4l*$^{f/f}$ *Villin*^{Cre} mice compared to *Nedd4l*$^{f/f}$ littermates. Furthermore,
239 the *Nedd4l*$^{f/f}$ *Villin*^{Cre} mice displayed higher serum FITC-dextran concentrations after DSS
240 treatment than *Nedd4l*$^{f/f}$ mice, while displaying similar epithelial permeability to *Nedd4l*$^{f/f}$
241 mice in the absence of DSS treatment (Figure 4B). Additionally, histopathological analysis,
242 tight junction protein 1 (ZO-1) immunofluorescence (IF) staining showed that *Nedd4l*

243 deficiency led to a more severe diminished expression of ZO-1 in the mucosal epithelium
244 in response to DSS treatment (Figure 4C).

245 To further explore the regulation of barrier integrity during the induction of colitis by
246 IEC-derived *Nedd4l*, the IECs from *Nedd4l*$^{f/f}$ *Villin*^{Cre} mice and *Nedd4l*$^{f/f}$ littermates with or
247 without DSS treatment were subjected to quantitative ubiquitination mass spectrometry
248 (MS) analysis. As shown in Supplemental Figure 4A, the Gene Ontology (GO) analysis
249 showed that the marked changed potential substrates mainly regulated protein localization,
250 transport, and transport activity. The Kyoto Encyclopedia of Genes and Genomes (KEGG)
251 analysis showed that protein digestion and absorption, mineral absorption, and ferroptosis
252 signaling pathways were markedly enriched in IECs from *Nedd4l*$^{f/f}$ *Villin*^{Cre} mice compared
253 to *Nedd4l*$^{f/f}$ mice (Figure 4D and Supplemental Figure 4B). In comparison with WT
254 littermates, the levels of TUNEL-positive epithelial cells, as well as the lipid peroxidation
255 measured by 4 hydroxynonenal (4-HNE)-positive staining cells, and malondialdehyde
256 (MDA) contents, were remarkably enhanced in DSS-treated *Nedd4l*$^{f/f}$ *Villin*^{Cre} mice,
257 suggesting that *Nedd4l* deficiency in IECs promoted the lipid peroxidation-mediated IEC
258 death after DSS treatment (Figure 4, E-I). IECs from *Nedd4l*$^{f/f}$ *Villin*^{Cre} mice exhibited much
259 more severe ferroptosis morphology, characterized by mitochondrial fragmentation, the
260 disappearance of internal cristae and collapse, compared with *Nedd4l*$^{f/f}$ mice (Figure 4J).
261 Consistently, the expression levels of ferroptosis and pro-inflammatory-related genes, such
262 as *Gpx4*, were significantly restricted in *Nedd4l*$^{f/f}$ *Villin*^{Cre} mice relative to *Nedd4l*$^{f/f}$ mice,
263 while the gene expression levels of transferrin receptor protein 1 (*TfR1*, also known as
264 *Tfrc*), prostaglandin-endoperoxide synthase 2 (*Ptgs2*), and lipocalin 2 (*Lcn2*) were

significantly increased in *Nedd4l*$^{f/f}$ *Villin*^{Cre} mice (Supplemental Figure 4, C and D). Furthermore, we stimulated the intestine organoids derived from *Nedd4l*$^{f/f}$ *Villin*^{Cre} mice and *Nedd4l*$^{f/f}$ mice with DSS and ferroptosis inducers in vitro, including Erastin, Erastin2 (a specific glutamine/cystine transporter inhibitor), and RSL3, to check if NEDD4L could mediate IEC ferroptosis. As shown in Figure 4, K and L, *Nedd4l* deficiency in IECs promoted lipid peroxidation-mediated IEC death, which was assessed by 4',6-diamidino-2-phenylindole (DAPI, indicating the dead cell) and fluorescein isothiocyanate (FITC)-BODIPY C11 staining (indicating intercellular lipid peroxidation production). Our data suggest that NEDD4L maintained intestinal barrier integrity by inhibiting IEC ferroptosis.

We have noticed that the expression of both the NEDD4L gene and protein were inhibited during the induction of colitis by DSS treatment in mice, indicating that DSS-induced IEC ferroptosis may be a potential inducer of the inhibition of NEDD4L expression during the colitis. Thus, ferroptosis inducers, including Erastin and RSL3, were employed to clarify the role of ferroptosis in NEDD4L expression. As shown in Supplemental Figure 4, E and F, Erastin and RSL3 significantly inhibited the NEDD4L protein expression, suggesting that cell ferroptosis may regulate NEDD4L expression. What's more, other classical cell death, TNF-α plus CHX-induced epithelial cell pyroptosis, and staurosporine-induced cell apoptosis inhibited the NEDD4L expression, except for insensitive necroptosis in HCT116 cells induced by T/S/Z (32-35) (Supplemental Figure 4, G and H). The key cytokines involved in colitis, such as TNF-α, IL-17A, and IL-1α, were employed to test if DSS-induced downstream cytokines restricted the NEDD4L expression. As shown in Supplemental Figure 4, I and J, TNF-α, but not IL-17A or IL-1α, restricted NEDD4L

expression in HCT116 cells along with NF-κB P65 subunit phosphorylation, indicating that TNF-α servers as the key mediator for inhibiting NEDD4L expression in IECs. Collectively, our data demonstrate that IEC death induced by the DSS, Erastin, RSL3, and downstream TNF-α inhibited NEDD4L expression.

Since DSS and ferroptosis inducers directly inhibited NEDD4L expression in HCT116 cells, we tested whether NEDD4L could regulate cell ferroptosis induced by DSS or ferroptosis inducers in vitro. As shown in Supplemental Figure 5, A-E, NEDD4L negatively regulated DSS-induced cell ferroptosis in HCT116 cells in an E3 ligase activity-dependent manner, as assessed by measurement of cell viability, lipid peroxidation, and MDA content. Similar phenotypes were also detected in other cell lines, including SW480 and RKO cells, using a siRNA silencing system (Supplemental Figure 5, F-K). Furthermore, *NEDD4L* deficiency in HCT116, SW480, and RKO cells significantly promoted Erastin- or RSL3-induced cell ferroptosis and lipid peroxidation production (Supplemental Figure 5, L-S). Collectively, these data further confirm that NEDD4L negatively regulated cell death and lipid peroxidation production mediated by DSS and ferroptosis inducers in multitype cell lines, in a manner dependent on its E3 ligase activity.

SLC3A2 is a potential substrate of NEDD4L in DSS-induced colitis

Based on the quantitative ubiquitylation MS analysis, SLC3A2, a transmembrane protein, which forms the key glutamine/cystine transporter with SLC7A11 and consequently participates in ferroptosis, was identified as one of the most remarkably ubiquitinylated substrates and was significantly downregulated in *Nedd4l*$^{f/f}$*Villin*^{Cre} IECs compared to that in *Nedd4l*$^{f/f}$ IECs after DSS challenge. Nevertheless, the fold change of SLC3A2 analyzed

by ubiquitylation MS was inhibited due to the reduced NEDD4L expression upon DSS treatment compared with untreated mice (Figure 5, A and B and Supplemental Figure 6, A and B). The interaction MS analysis in Flag-NEDD4L stably expressed HCT116 cells indicated that NEDD4L interacted with SLC3A2 (Figure 5B and Supplemental Figure 6C). Based on the combined analysis of quantitative ubiquitination MS and interaction MS, we hypothesized that NEDD4L might interact with SLC3A2 and regulate its ubiquitination, triggering IEC ferroptosis and aggravating DSS-induced colitis. Consistently, the protein expression of SLC3A2 was significantly downregulated in IECs of *Nedd4l*$^{f/f}$ *Villin*^{Cre} mice compared to that of *Nedd4l*$^{f/f}$ mice (Supplemental Figure 6D). Whereas, *Nedd4l* deficiency in IECs had no effects on the protein expressions of GP130 and MEKK2, which have been identified to be potential substrates of NEDD4L in other cells (29, 30). Furthermore, upon DSS treatment, the expression of SLC3A2 was also downregulated in IECs of *Nedd4l*$^{f/f}$ *Villin*^{Cre} mice compared to that of *Nedd4l*$^{f/f}$ mice (Figure 5C). Based on the ubiquitylation MS analysis, we found that NEDD4L protein abundance was positively correlated with SLC3A2 protein abundance, further indicating the probability of SLC3A2 as the potential substrate of NEDD4L (Supplemental Figure 6E). It has been reported that SLC3A2 regulates the expression of CyclinD1 in IECs to participate in mouse colitis(36). However, we did not observe any difference in the gene expressions of *Cyclind1* and *Slc3a2* in *Nedd4l*$^{f/f}$ *Villin*^{Cre} and *Nedd4l*$^{f/f}$ mice (Supplemental Figure 6F). In addition, we revealed that *Nedd4l* deficiency in IECs restricted SLC3A2 and GPX4 protein expression (Figure 5, C-E). DSS treatment significantly inhibited the protein expression levels of GPX4, SLC3A2, and NEDD4L. Furthermore, the protein expression levels of both NEDD4L and GPX4 were

positively correlated with SLC3A2 in IECs upon DSS treatment (Supplemental Figure 6, G-I). Importantly, the protein expression level of NEDD4L in patients with IBDs was positively correlated with SLC3A2 (Figure 5, F and G).

NEDD4L knockout in intestinal organoids and HCT116 cells impaired DSS-induced SLC3A2 and GPX4 expression but increased the TFRC expression, enhancing cell ferroptosis (Figure 5, H and I). NEDD4L positively regulated SLC3A2 and GPX4 protein expression in HCT116 cells in its E3 ubiquitin ligase activity-dependent manner (Figure 6J). Similar results were observed in a multitype of DSS-, Erastin-, or RSL3-treated intestinal cell lines, such as HCT116, SW480, and RKO cells, using a siRNA silencing system (Figure 5, K-M and Supplemental Figure 6, J-M).

As a potential substrate of NEDD4L in ferroptosis signaling, SLC3A2 was poorly studied (11). Therefore, we determined whether SLC3A2 could regulate cell ferroptosis and signaling transduction mediated by DSS or ferroptosis inducers. As shown in Figure 6, A-I and Supplemental Figure 7, A-I, silencing of endogenous *SLC3A2* significantly promoted cell death and lipid peroxidation production induced by DSS and ferroptosis inducers. Additionally, silencing of endogenous *SLC3A2* inhibited GPX4 expression but enhanced TFRC expression after DSS or ferroptosis inducer treatment compared with scramble siRNA (si*NC*)-transfected cells. Overexpression of exogenous *SLC3A2* in HCT116 cells inhibited DSS-induced cell death and production of lipid peroxidation by upregulating the GPX4 expression (Figure 6, J-M), indicating that SLC3A2 negatively regulated cell ferroptosis mediated by DSS and ferroptosis inducers in vitro. Furthermore, overexpression of the exogenous *SLC3A2* eliminated the difference in DSS-induced cell

death, production of lipid peroxidation, and protein expression levels of GPX4 and TFRC between *NEDD4L*-silenced and scramble siRNA (si*NC*)-transfected HCT116 cells (Figure 6, N-P). Collectively, these data suggest that NEDD4L regulated DSS-induced cell ferroptosis through the SLC3A2-GPX4 axis.

NEDD4L mediates SLC3A2 ubiquitination

To determine the mechanism through which NEDD4L orchestrates SLC3A2 protein expression, we investigated the interaction between NEDD4L and SLC3A2 in HCT116 and HEK293T cells. As shown in Figure 7, A and B, NEDD4L interacted dynamically with SLC3A2 upon DSS treatment, peaking at 12 hours. The E3 ligase activity mutant of NEDD4L (NEDD4L-C942A or NEDD4L-CA) abolished this interaction. To map the domains required for NEDD4L to interact with SLC3A2, we constructed a series of plasmids expressing wild-type or mutant NEDD4L, in which C2 (ΔC2), WW (ΔWW), or HECT (ΔHECT) domain was deleted, respectively. As shown in Figure 7C, the deletion of the HECT domain but not the C2 and WW domain disrupted the interaction between NEDD4L and SLC3A2, demonstrating that the HECT domain was necessary for NEDD4L to bind SLC3A2. As an E3 ubiquitin ligase, NEDD4L might regulate the stability of the SLC3A2 protein by mediating its ubiquitination. Firstly, we used the ubiquitin (Ub) antibody to immunoprecipitate endogenous Ub to compare the amount of poly-Ub-linked SLC3A2 in WT (sg*NTC*) or NEDD4L knockout (sg*NEDD4L*) HCT116 cells. As shown in Figure 7D, NEDD4L knockout in HCT116 cells impaired the poly-Ub-linked SLC3A2 upon DSS treatment, consistent with the phenotype observed in our ubiquitination MS in IECs. Then, we performed ubiquitination assays in HEK293T cells. As shown in Figure 7E and

375 Supplemental Figure 8A, NEDD4L positively regulated the poly-ubiquitination of SLC3A2.
376 Furthermore, in vitro cell-free ubiquitination assays demonstrated that it was the wild-type
377 NEDD4L protein, but not the NEDD4L-C942A protein, that directly promoted the poly-
378 ubiquitination of SLC3A2 (Figure 7F). Following MG132 treatment, but not bafilomycin A1
379 (Baf A1) treatment, the expression of SLC3A2 in wild-type NEDD4L transfected cells was
380 reduced to the level comparable with that in control or NEDD4L-CA mutant transfected
381 HCT116 cells, suggesting that NEDD4L regulated the stability of SLC3A2 protein by
382 mediating SLC3A2 ubiquitination in a proteasome-dependent manner (Supplemental
383 Figure 8B). Notably, NEDD4L overexpression in HCT116 cells markedly enhanced the
384 protein stability of SLC3A2 compared to that in NEDD4L-C942A or control transfected cells
385 (Supplemental Figure 8C). NEDD4L-ΔHECT completely lost the capability to mediate
386 SLC3A2 ubiquitination (Figure 7G), suggesting that the HECT domain of NEDD4L was
387 critical for its interaction with and ubiquitination of SLC3A2. Furtherly, NEDD4L mainly
388 promoted Lys-63(K63O)-linked poly-ubiquitination of SLC3A2 (Figure 7G), which is
389 consistent with the well-established notion that the C-terminal amino acids determine the
390 ubiquitin chain specificity of the HECT-type E3 ligases and NEDD4 family ligases, including
391 NEDD4L, which exhibit strict specificity towards K63 linkages (37). NEDD4L knockout
392 markedly impaired DSS-induced K63-linked poly-ubiquitination of SLC3A2, but enhanced
393 K48-linked poly-ubiquitination of SLC3A2, resulting in a reduced SLC3A2 protein
394 expression compared to sg*NTC* HCT116 cells (Figure 7I). Furthermore, NEDD4L promoted
395 K63-linked poly-ubiquitination of SLC3A2 in a dosage-dependent manner and inhibited the
396 K48-linked poly-ubiquitination of SLC3A2 in HEK293T cells (Figure 8J). We also found that

SLC3A2 interacted with GPX4. However, NEDD4L neither interacted with nor ubiquitylated GPX4(Supplemental Figure 8, D and E). These data suggest that NEDD4L mediated the K63-linked poly-ubiquitination of SLC3A2, but not of GPX4.

Nedd4l deficiency promotes colitis pathogenesis via ferroptosis in mice

To further determine whether NEDD4L regulates colitis through the ferroptosis pathway, colonic tissues from *Nedd4l*$^{f/f}$*Villin*^{Cre} and *Nedd4l*$^{f/f}$ mice treated with DSS were subjected to RNA-sequencing to explore the underlying mechanisms. KEGG analysis revealed that cytokine-cytokine receptor interaction and IL-17 signaling pathway were the top 2 pathways up-regulated in colonic tissues from *Nedd4l*$^{f/f}$*Villin*^{Cre} mice compared to *Nedd4l*$^{f/f}$ mice (Supplemental Figure 9A). GO analysis showed that the cellular intrinsic apoptotic signaling and regulation of the hydrogen peroxide metabolic process were significantly upregulated in colonic tissues from *Nedd4l*$^{f/f}$*Villin*^{Cre} mice compared to *Nedd4l*$^{f/f}$ mice (Supplemental Figure 9B), suggesting that cell death and peroxidation may be involved in NEDD4L-mediated colitis. Previous studies have shown that NEDD4L regulated IL-17-induced inflammatory response through MEKK2 (29). Since IL-17R signaling can affect intestinal epithelial cell homeostasis, differentiation, and tumor development(38-40), we tested whether NEDD4L regulates DSS-induced colitis through IL-17R signaling by using an IL-17 neutralizing antibody. As shown in Supplemental Figure 9, C-F, the IL-17 neutralizing antibody treatment successfully inhibited DSS-mediated colitis in WT mice but did not eliminate the colitis phenotype difference induced by *Nedd4l* deficiency. Although Syk is known to be a target for NEDD4L in mast cells(41), continual intraperitoneal(*i.p.*) injection of a Syk-specific inhibitor, BAY 61-3606, during colitis induction did not eliminate

419 the colitis phenotype difference between *Nedd4l*$^{f/f}$*Villin*^{Cre} and *Nedd4l*$^{f/f}$ mice (Supplemental
420 Figure 9, G-J). However, treatment with a lipid peroxidation scavenger, N-acetylcysteine
421 (NAC), significantly attenuated the development of colitis in *Nedd4l*$^{f/f}$ *Villin*^{Cre} mice. More
422 importantly, NAC treatment rescued the colitis phenotype in *Nedd4l*$^{f/f}$*Villin*^{Cre} to a
423 comparable level with those in *Nedd4l*$^{f/f}$ mice (Supplemental Figure 9, K-N).

424 To further explore if NEDD4L regulates colitis via ferroptosis, a ferroptosis-specific
425 inhibitor, ferrostatin-1 (Fer-1), was continual *i.p.* injected during DSS-induced colitis in
426 *Nedd4l*$^{f/f}$*Villin*^{Cre} and *Nedd4l*$^{f/f}$ mice. As shown in Figure 8, A-J and Supplemental Figure 10,
427 A and B, Fer-1 markedly rescued the colitis phenotype in DSS-induced *Nedd4l*$^{f/f}$*Villin*^{Cre}
428 mice to levels comparable to those in Fer-1-treated *Nedd4l*$^{f/f}$ mice, as characterized by
429 reduced diarrhea and rectal bleeding, decreased colon shortening, less epithelial damage,
430 and decreased crypt architecture disruption, decreased epithelial cell death, reduced lipid
431 peroxidation production, and decreased inflammatory cytokines, but increased tight
432 junctions. Furthermore, continual *i.p.* injection of Fer-1 during the induction of colitis
433 eliminated the difference in colitis phenotype between *Nedd4l*$^{f/f}$*Villin*^{Cre} and *Nedd4l*$^{f/f}$ mice.
434 The difference in the expression of ferroptosis-related genes (including *Gpx4*, nuclear
435 receptor coactivator 4 (*Ncoa4*), acyl-CoA synthetase family member 2 (*Acsf2*), and acyl-
436 CoA synthetase long chain family member 4 (*Acsl4*)) and proteins (including GPX4,
437 SLC3A2, and TFRC) between *Nedd4l*$^{f/f}$*Villin*^{Cre} and *Nedd4l*$^{f/f}$ mice were eliminated by the
438 treatment of Fer-1 (Figure 8, K-M). Additionally, treatment with another ferroptosis inhibitor
439 deferoxamine mesylate (DFOM, a ferric ion depletion reagent) during the DSS
440 administration eliminated the colitis phenotype difference in mice (Supplemental Figure 10,

C-K). These data suggest that *Nedd4l* deficiency in IECs promoted the pathogenesis of colitis in a ferroptosis-dependent manner.

Gut microbiota involves in NEDD4L-regulated colitis

The gut microbiota is critical for maintaining gut homeostasis. To further evaluate if the exacerbated colitis in *Nedd4l*-deficient mice compared to control littermates is microbiota-dependent, we co-housed the *Nedd4l*-deficient mice with control littermates for 2 weeks before DSS administration. As shown in Supplemental Figure 11, A-F, co-housing eliminated the development of more severe DSS-induced colitis in *Nedd4l*-deficient mice compared to co-housed control littermates, indicating that NEDD4L protects against colitis in a manner dependent on the gut microbiota. To demonstrate how the microbiota regulates DSS-induced colitis in mice, feces from *Nedd4l*$^{f/f}$*Villin*^{Cre} mice and the control littermates, treated with or without DSS, were collected and then subjected to 16s rDNA sequencing. As shown in Supplemental Figure 11G, the abundance of *Akkermansia* was markedly increased, while the abundances of *Bifidobacterium* and *Lactobacillus* were markedly diminished in *Nedd4l*$^{f/f}$ *Villin*^{Cre} mice compared to *Nedd4l*$^{f/f}$ mice after administration of DSS, with similar abundances in untreated mice. As important commensal intestinal bacteria, *Akkermansia, Bifidobacterium,* and *Lactobacillus* play pivotal roles in maintaining intestinal homeostasis(2). However, an abnormally increased abundance of *Akkermansia* could promote the degradation of intestinal mucin, thus exacerbating colitis in mice (42), which is consistent with our phonotype that *Nedd4l*$^{f/f}$ *Villin*^{Cre} mice exhibited less intestinal mucin production after DSS treatment visualized by AB-PAS staining of the colon sections (Supplemental Figure 11H). To further investigate the involvement of gut microbiota in

NEDD4L-regulated colitis, antimicrobial peptides of the small intestine were detected in untreated and DSS-treated *Nedd4l*$^{f/f}$ *Villin*^{Cre} mice and *Nedd4l*$^{f/f}$ mice. As shown in Supplemental Figure 11, I and J, *Nedd4l* deficiency in mice initially had no effect on the antimicrobial peptide expression without DSS treatment, such as angiogenin, ribonuclease A family, member 4 (*Ang4*), defensin, alpha, 29 (*Defa-rs1*), and defensin, alpha, 20 (*Defa20*). DSS treatment resulted in intestinal epithelial cell damages along with decreased antimicrobial peptide gene expression patterns. What's more, *Nedd4l* deficiency in IECs significantly impaired antimicrobial peptide expression in *Nedd4l*$^{f/f}$ *Villin*^{Cre} mice than in *Nedd4l*$^{f/f}$ mice, suggesting a much stronger impact, such as IEC death, plays a critical role during the DSS-induced colitis. Thus, single-housed *Nedd4l*$^{f/f}$ *Villin*^{Cre} and *Nedd4l*$^{f/f}$ mice were gavaged with *Bifidobacterium* and *Lactobacillus* (*Bif&Lac,* 1x10^{8}CFU/mice daily) during the induction of colitis. Interestingly, as shown in Supplemental Figure 11, K-N, oral administration of *Bifidobacterium* and *Lactobacillus* significantly restricted colitis development in both *Nedd4l*$^{f/f}$ *Villin*^{Cre} mice and *Nedd4l*$^{f/f}$ mice, characterized by a lower degree of the inflammatory syndrome and stronger mucus secretion ability compared with DSS-treated single-housed *Nedd4l*$^{f/f}$ *Villin*^{Cre} mice without bacteria gavage, indicating that the intestinal microbiota involved in NEDD4L-regulated colitis, particularly *Bifidobacterium* and *Lactobacillus.* The IEC samples isolated from the bacteria gavage mice revealed that the administration of microbiota significantly promoted GPX4 and SLC3A2 expression but impaired TFRC expression, thus eliminating the signaling difference between *Nedd4l*$^{f/f}$ *Villin*^{Cre} and *Nedd4l*$^{f/f}$ mice (Supplemental Figure 11, O and P), indicating a protective role of gut microbiota in inhibiting ferroptosis through GPX4(43).

485 **_Nedd4l_ deficiency promotes the pathogenesis of CAC in mice**

486 AOM/DSS-induced colitis-associated colorectal cancer (CAC) model in mice has been
487 widely used for research on inflammation-related cancer in mice, as mice with more severe
488 inflammation are more likely to develop colorectal cancer (44, 45). Therefore, we further
489 explored the regulatory role of NEDD4L in CAC using *Nedd4l* global deficiency mice and
490 *Nedd4l*$^{f/f}$*Villin*^{Cre} mice. In vivo, magnetic resonance images (MRI) analysis revealed a
491 marked increase in colon distension of *Nedd4l*$^{f/f}$*Villin*^{Cre} mice in both axial and coronal
492 images, and a higher number of tumors in the colons of *Nedd4l*$^{f/f}$*Villin*^{Cre} mice compared to
493 WT mice on day 90 (Figure 9A). As shown in Figure 9, A-D and Supplemental Figure 12,
494 A-C, *Nedd4l*-deficient mice were more susceptible to cancer. Compared to their wild-type
495 littermates, we found higher levels of Ki67^{+} cells per crypt in the adjacent tumor and tumor
496 tissues from *Nedd4l*$^{+/-}$ and *Nedd4l*$^{f/f}$*Villin*^{Cre} mice following AOM/DSS treatment (Figure 9,
497 E and F and Supplemental Figure 12, D-E), as well as increased lipid peroxidation
498 production in tumor tissues of *Nedd4l*$^{f/f}$*Villin*^{Cre} mice (Figure 9G). Since NEDD4L regulates
499 the IEC inflammation through ferroptosis signaling, we hypothesized that NEDD4L may
500 regulate CAC through ferroptosis signaling. To test this hypothesis, a ferroptosis inhibitor,
501 DFOM, was *i.p.* injected during DSS treatment as indicated in Figure 9H, to inhibit the
502 inflammatory response. As shown in Figure 9, I-L, DFOM treatment significantly inhibited
503 AOM/DSS-induced tumor formation and lipid peroxidation in *Nedd4l*$^{f/f}$*Villin*^{Cre} mice
504 compared to the ddH_2O-treated control mice, and further eliminated the phenotype
505 difference between *Nedd4l*$^{f/f}$*Villin*^{Cre} mice and *Nedd4l*$^{f/f}$ mice, suggesting that NEDD4L
506 regulated CAC through ferroptosis signaling.

Lipid peroxidation during colitis promotes the pathogenesis of CAC, making colitis a risk factor for colorectal cancer (46-48). Next, we aimed to explore the changes in the NEDD4L gene or protein during CAC. According to the TCGA and GEO data, the *NEDD4L* gene was significantly downregulated in the tumor tissues of patients with colorectal cancer and in the tissues from CAC mice compared to their normal tissues (Supplemental Figure 13, A and B). The expression of NEDD4L dynamically changed during the AOM/DSS induction. NEDD4L gene and protein showed no significant changes on the 15^{th} day after the AOM/DSS induction but were slightly downregulated on the 60^{th} day when the mice had minor epithelial hyperplasia/ dysplasia. Moreover, the gene and protein levels of NEDD4L were significantly downregulated on the 90^{th} day after the AOM/DSS induction, when the mice had obvious neoplasia formation (Figure 10, A-C and Supplemental Figure 13, C and D). The protein expression of NEDD4L was significantly correlated with both SLC3A2 and GPX4 during the induction of mice CAC (Figure 10 D). NEDD4L expression was significantly inhibited in IECs of adjacent tumor and tumor tissues from CAC mice compared to the distal normal colon (Supplemental Figure 13, E-G). This suggested that the inhibited NEDD4L expression was a consequence of dysregulated intestinal homeostasis, including inflammation damage and tumor formation. Furthermore, NEDD4L expression was negatively correlated with the survival outcomes, and was significantly reduced in advanced tumor stages (Supplemental Figure 13, H-J). Using tissue microarray (TMA)-based IHC of colon sections from patients with colorectal cancer, we found that protein expression of NEDD4L was significantly inhibited in IECs of colonic tumor tissues compared with normal tissues. Meanwhile, lipid peroxidation was significantly enhanced in

IECs from tumor and adjacent-tumor tissues compared to the normal tissues (Figure 10, E and F), consistent with the notion that 4-HNE promotes the development of colorectal cancer (46). Moreover, the protein expression of NEDD4L was positively correlated with SLC3A2 and GPX4 in the IECs of patients with colorectal cancer (Figure 11, G and H). Consistently, we found that the gene expression of SLC3A2 was significantly correlated with that of GPX4, but not with NEDD4L, in the GEPIA2 database, suggesting a posttranslational modification of NEDD4L on SLC3A2 (Supplemental Figure 13, K and L). Collectively, our data support the notion that the protective role of NEDD4L in the pathogenesis of AOM/DSS-induced colorectal cancer in mice was dependent on its controlling SLC3A2/GPX4 axis.

Discussion

NEDD4L is a conserved HECT E3 ligase highly expressed in human neurons, the lung, and intestinal systems. It is known to regulate the ubiquitination of membrane proteins (21). Herein, we demonstrated that both the gene and protein levels of NEDD4L were significantly downregulated in IECs from patients with IBDs and colorectal cancer. The expression level of NEDD4L was negatively correlated with the disease status of colitis. Additionally, *Nedd4l* deficiency in mice significantly promoted the pathogenesis of colitis and AOM/DSS-induced tumorigenesis.

IEC death is thought to be the main pathological mechanism of dysregulated intestinal homeostasis (13). It has been widely recognized that IEC death induced by apoptosis, necroptosis, and pyroptosis is the first step leading to the destruction of intestinal barrier integrity, thus initiating intestinal mucosa inflammation and resulting in IBDs (1, 3). Therefore, exploring functional proteins involved in maintaining intestinal barrier integrity is of great significance for the early diagnosis and treatment of IBDs. Ferroptosis is a recently defined form of cell death involving lipid peroxidation and iron (Fe). There are some clues that ferroptosis occurs in DSS-induced colitis and IBD and may contribute to their pathogenesis(10, 49, 50). In our study, *Nedd4l*-global deficiency in mice exacerbated DSS-induced colitis compared to the WT mice. Further bone marrow chimera experiments demonstrated that *Nedd4l* deficiency in non-bone marrow cells aggravated DSS-induced colitis, suggesting an important role of NEDD4L in non-bone marrow cells. Goblet cells are the most abundant cells in the intestine and NEDD4L is highly expressed in goblet cells but downregulated in IECs of patients with IBDs, thus we employed the *Nedd4l* IEC knock-

573 out mice to investigate the function of NEDD4L in IECs in colitis. Consistently, *Nedd4l*
574 deficiency in IECs strongly exacerbated DSS/TNBS-induced colitis and AOM/DSS-induced
575 CAC. Further mechanism studies revealed that *Nedd4l* deficiency in IECs induced more
576 severe IEC death and damage of the intestinal barrier through promoting IEC ferroptosis
577 compared with WT mice upon DSS treatment, suggesting that the damaged intestinal
578 barrier integrity served as the initiation factor for NEDD4L to modulate DSS-induced colitis.
579 Intestine is a complex organ composed of many cells, including non-bone marrow-derived
580 cells, such as IECs, mesenchymal cells, endothelial cells, as well as bone marrow-derived
581 cells, including macrophages, monocytes, dendritic cells (DCs), lymphocytes, and even
582 innate lymphoid cells (ILCs), maintaining the intestinal homeostasis through a complex
583 regulatory network. According to scRNA-seq data, *NEDD4L* gene was lowly expressed in
584 bone-marrow-derived and non-bone-marrow-derived cells, thus indicating a potentially
585 limited regulatory function for NEDD4L in these cells.

586 NEDD4L expression was reported to be downregulated in many tumors and psoriasis,
587 suggesting a potential biomarker for diseases (30, 51, 52). In our study, we demonstrated
588 that both the NEDD4L gene and protein were downregulated in IECs of patients with colitis
589 or CAC, and this downregulation was correlated with the disease status of colitis and
590 survival outcomes of colorectal cancer. Our in vitro cellular data indicated that NEDD4L
591 expression was affected by many pathways ending in cell death and TNF-α. However, due
592 to the lack of clinical IBD biopsies from patients with infectious or diverticulitis, we cannot
593 get the conclusion that NEDD4L expression would be inhibited in any inflammatory setting.
594 As colitis develops, intestinal lamina propria infiltrates immune cells secret cytokines,

595 particularly TNF-α, a pivotal mediator of inflammation and cell death, and it is also a key
596 therapeutic target in IBD treatment. As predicted based on our in vitro cell line data, TNF-
597 α may impair the expression of NEDD4L in IECs, further amplifying the inflammatory
598 signaling and enhancing cell death in vivo, resulting in aggravated inflammation and
599 epithelial barrier integrity damage, ultimately leading to IBDs. Thus, NEDD4L may act as a
600 general homeostatic regulator of the epithelial barrier integrity that could be at a common
601 point in many TNF-α-related pathways that converge to mediate cell injury and death.
602 Accumulating evidence suggests that epigenetic modifications, such as chromatin
603 remodeling or DNA methylation, which occur in response to pathological environmental
604 stimuli, contribute to tissue-specific and disease-associated effects mediated by TNF-α(53).
605 Our previous data has demonstrated that NEDD4L expression could be modulated by the
606 IMQ-induced EZH2/H3K27me3 axis in keratinocytes(30). However, it remains to be
607 determined whether the transcriptional regulation of NEDD4L during intestinal injury or cell
608 death is induced by TNF-α-mediated histone methylation, which could be further explored.
609 The ubiquitin-proteasome system (UPS) is a highly finely modulated protein regulation
610 system, which is important for cell proliferation, apoptosis, immunity, and development (54-
611 56), thus regulating inflammatory diseases, tumors, and cardiovascular diseases (54).
612 Based on our unbiased ubiquitinoylation MS sequencing, the ferroptosis signaling pathway
613 was substantially enriched in IECs of DSS-treated *Nedd4l*-deficient mice. Our further
614 biochemistry experiment demonstrated that NEDD4L bound to SLC3A2 and promoted the
615 K63-linked ubiquitinoylation while inhibiting the K48-linked ubiquitinoylation of SLC3A2,
616 positively regulating the protein stability of SLC3A2, thus inhibiting the IEC ferroptosis.

Domain mapping data identified that the HECT domain of NEDD4L was required for interaction with and ubiquitinoylation of SLC3A2. Our data suggested that SLC3A2 could be the potential target of NEDD4L in IECs, which seems inconsistent with the reported notion that SLC3A2 (CD98) positively regulates intestinal homeostasis by modulating mβ1-integrin signaling in IECs (36). However, our in vivo and in vitro data demonstrated that SLC3A2 interacted with GPX4, and its protein expression was positively correlated with that of GPX4, but not with CyclinD1, partly consistent with reported data that SLC3A2 is positively correlated with GPX4(57, 58). Furthermore, ferroptosis-specific inhibitors, Fer-1 and DFOM, or a lipid peroxidation scavenger, NAC, eliminated the phenotypic difference of DSS-induced colitis between Nedd4l IEC-deficient mice and WT mice. In contrast, other NEDD4L potential target signaling-related inhibitors, such as BAY 61-3606 and anti-IL17 neutralizing antibody, could not eliminate the phenotypic difference of DSS-induced colitis. Collectively, our in vitro and in vivo data suggest that NEDD4L modulated SLC3A2 ubiquitinoylation to regulate DSS-induced colitis. Further mechanisms need to be explored to clarify the complicated functions of SLC3A2 both in mβ1-integrin signaling and ferroptosis signaling.

Our study revealed a positive correlation between NEDD4L protein expression and SLC3A2 in humans with IBDs and colorectal cancer, demonstrating that NEDD4L/SLC3A2/GPX4 axis played an important role in colitis and CAC. IL-17R- signaling can affect intestinal epithelial cell homeostasis, differentiation, and tumor development(38-40). However, our data demonstrated that NEDD4L regulated DSS-induced colitis in an IL-17R signaling-independent manner. As colitis is a risk factor, and the AOM/DSS model

mice have more severe inflammation, which would drive more serious cancer regardless of any cell-intrinsic effect (44, 45), suggesting that blocking IL-17R- signaling may have no influence on CAC mediated by the *Nedd4l* IEC deficiency. It has been demonstrated that NEDD4 and NEDD4L knockout in IECs regulated the Lgr5 degradation to mediate Wnt signaling and cancer development in APC^{min} mice (27, 60). In addition, a prior study has implicated NEDD4 in mediating Nrf2 to regulate HO-1- and DSS-induced colitis (61, 62). In epithelial cells, E-cadherin suppresses ferroptosis by activating the intracellular NF2 (also known as merlin) and Hippo signaling pathway (63). Merlin/NF2, a key activator of the Hippo pathway in growth control and regarded as a key tumor suppressor, is regulated by phosphorylation. However, Merlin ubiquitination is mediated by the E3 ubiquitin ligase NEDD4L, which requires a scaffold protein, AMOTL1, to interact with Merlin (64). Thus, these data suggest a potential role of NEDD4 or NEDD4L in epithelial cell inflammation and cell proliferation-involved colitis or CRC. However, our unbiased ubiquitinoylation MS sequencing data and in vivo experiments support that SLC3A2/GPX4-mediated lipid peroxidation production signaling played a dominant role in controlling colitis and CAC. Whether NEDD4L regulates the Lgr5/Wnt signaling or NF2/Yap signaling to control CAC remains to be further studied using their specific inhibitors or genetic knockout mice for the CAC model.

The gut microbiota is a key factor of colitis that may directly affect the pathogenesis of colitis (2, 59). In our study, co-housed breeding of *Nedd4l*-deficient and WT mice developed comparable severities of DSS-induced colitis, suggesting that gut microbiota plays a pivotal role in NEDD4L-regulated colitis. Further analysis, including 16S rDNA-sequencing of the

feces and in vivo supplement of commensal intestinal bacteria, revealed that the *Lactobacillus* and *Bifidobacterium* were critical for NEDD4L-regulated colitis. Our signaling study demonstrated that supplementation of *Lactobacillus* and *Bifidobacterium* blocked the GPX4-mediated ferroptosis signaling, suggesting an important role of these gut microbiota in ferroptosis-mediated colitis.

In conclusion, our study demonstrated a significant reduction in the expression of the E3 ubiquitin ligase NEDD4L in IECs of patients with IBDs and colorectal cancer. Additionally, *Nedd4l* knockout in mice significantly enhanced DSS/TNBS-induced colitis and AOM/DSS-induced CAC by triggering SLC3A2-mediated ferroptosis (Graphical abstract). This study provides a potential diagnostic biomarker and clinical treatment target for inflammatory bowel diseases and CAC.

Methods

Sex as a biological variable

Our study utilized both male and female biopsies from humans and mice for the study, as sex was not considered a biological variable.

Animals

Heterozygous *Nedd4l* mice (on a BALB/cByJ background) were purchased from JAX® Mice, America. *NEDD4L*$^{f/f}$ mice (on a C57BL/6J background) were purchased from Cyagen Bioscience. Knockout (KO) mice and the *WT* littermate control mice were generated by crossing *Nedd4l* heterozygous. *Nedd4l* IEC-knockout mice were generated by crossing *Nedd4l*$^{f/f}$ mice with *Villin*^{Cre} mice (on a C57BL/6J background). All mice were maintained under the specific-pathogen-free (SPF) condition in the Laboratory Animal Center of Zhejiang University. Eight- to ten-week-old mice were studied using TNBS or DSS-induced colitis models as described previously(65). For inhibition experiments in vivo, the *Nedd4l*$^{f/f}$ *Villin*^{Cre} and corresponding control mice were daily treated with Fer1 (5 μmol/kg), DFOM (200mg/kg), NCA (300mg/kg), BAY 61-3066 (5 mg/kg), anti-IL17A antibody (100 μg/mouse), or corresponding control vehicle respectively, 3 days before 2% DSS administration until to the end of experiments.

Statistical analysis

The statistical analysis was performed using a log-rank test for survival two curves analysis, a two-way ANOVA test for two curves analysis, a Pearson correlation test for correlation analysis, or a 2-tailed unpaired Student's t-test for two groups analysis. When appropriate, the statistical significance of differences among multiple groups was analyzed using one-

way ANOVA with the Bonferroni correction. Differences were considered significant at $p<0.05$.

Study approval

Written patient consent was provided, and ethics approval for human samples was granted by the Medical Ethics Committee of Zhejiang University School of Medicine (ethics approval 2021-005, 20210125-30, IIT20240689BR) for harvesting human tissues. All animal research was performed under a protocol approved by the Medical Experimental Animal Care Commission of Zhejiang University (ethics approval 202118445, ZJU20240729).

Disclosure and Competing Interests Statement

The authors declare that they have no conflict of interest.

Data availability

Raw data of protein sequencing were deposited in iProX (https://www.iprox.cn/page/home.html) under accession no. PXD057172 and PXD057173. Raw data of RNA sequencing were deposited in GEO under accession no. GSE282883 and GSE282497. The values for all data points in the graphs are reported in the Supporting Data Values file. Additional methods are provided in the Supplemental material.

Author Contributions

J.L., W.L., N.W., Y.Y., H, W., X. A., H.LI., H.LUI., Y.J., and Y.W. performed experiments. J.L., W.L., and Y.J. performed the statistical analysis. X.C. and J.X. provided single cell analysis. X.L, J.L, and Z.X. provided some reagents. T.Z., X.W., and W.L. designed the study. J.L. and W.L. drafted the manuscript.

Acknowledgments

This work is supported by grants from the National Natural Science Foundation of China (82071774, 82171765, 81901595, 82371763), Zhejiang Province Natural Science Foundation project (LZ22H100001, LY22H100002), and the Science and Technology Bureau of Hangzhou, Zhejiang Province (20212013B05 to J.P. (Jianping Pan)). We thank Chun Guo, Jiajia Wang, Jingyao Chen, Shuangshuang Liu, and Yanwei Li from the Core Facilities, Zhejiang University School of Medicine for their technical support.

References

1. Peterson LW, and Artis D. Intestinal epithelial cells: regulators of barrier function and immune homeostasis. *Nat Rev Immunol.* 2014;14(3):141-53.

2. Thaiss CA, Zmora N, Levy M, and Elinav E. The microbiome and innate immunity. *Nature.* 2016;535(7610):65-74.

3. Turner JR. Intestinal mucosal barrier function in health and disease. *Nat Rev Immunol.* 2009;9(11):799-809.

4. Parikh K, Antanaviciute A, Fawkner-Corbett D, Jagielowicz M, Aulicino A, Lagerholm C, et al. Colonic epithelial cell diversity in health and inflammatory bowel disease. *Nature.* 2019;567(7746):49-55.

5. Jiang X, Stockwell BR, and Conrad M. Ferroptosis: mechanisms, biology and role in disease. *Nat Rev Mol Cell Biol.* 2021;22(4):266-82.

6. Wang W, Green M, Choi JE, Gijon M, Kennedy PD, Johnson JK, et al. CD8(+) T cells regulate tumour ferroptosis during cancer immunotherapy. *Nature.* 2019;569(7755):270-4.

7. Liang D, Minikes AM, and Jiang X. Ferroptosis at the intersection of lipid metabolism and cellular signaling. *Mol Cell.* 2022;82(12):2215-27.

8. Chen X, Kang R, Kroemer G, and Tang D. Broadening horizons: the role of ferroptosis in cancer. *Nat Rev Clin Oncol.* 2021;18(5):280-96.

9. Panda SK, Peng V, Sudan R, Ulezko Antonova A, Di Luccia B, Ohara TE, et al. Repression of the aryl-hydrocarbon receptor prevents oxidative stress and ferroptosis of intestinal intraepithelial lymphocytes. *Immunity.* 2023.

10. Xu M, Tao J, Yang Y, Tan S, Liu H, Jiang J, et al. Ferroptosis involves in intestinal epithelial cell

772 death in ulcerative colitis. *Cell Death Dis.* 2020;11(2):86.

773 11. Koppula P, Zhuang L, and Gan B. Cystine transporter SLC7A11/xCT in cancer: ferroptosis,
774 nutrient dependency, and cancer therapy. *Protein Cell.* 2021;12(8):599-620.

775 12. Bulek K, Zhao J, Liao Y, Rana N, Corridoni D, Antanaviciute A, et al. Epithelial-derived gasdermin
776 D mediates nonlytic IL-1beta release during experimental colitis. *J Clin Invest.*
777 2020;130(8):4218-34.

778 13. Patankar JV, and Becker C. Cell death in the gut epithelium and implications for chronic
779 inflammation. *Nat Rev Gastroenterol Hepatol.* 2020;17(9):543-56.

780 14. Bertrand MJ, Doiron K, Labbe K, Korneluk RG, Barker PA, and Saleh M. Cellular inhibitors of
781 apoptosis cIAP1 and cIAP2 are required for innate immunity signaling by the pattern
782 recognition receptors NOD1 and NOD2. *Immunity.* 2009;30(6):789-801.

783 15. Song H, Liu B, Huai W, Yu Z, Wang W, Zhao J, et al. The E3 ubiquitin ligase TRIM31 attenuates
784 NLRP3 inflammasome activation by promoting proteasomal degradation of NLRP3. *Nat*
785 *Commun.* 2016;7:13727.

786 16. Vereecke L, Vieira-Silva S, Billiet T, van Es JH, Mc Guire C, Slowicka K, et al. A20 controls
787 intestinal homeostasis through cell-specific activities. *Nat Commun.* 2014;5:5103.

788 17. Zhang H, Cui Z, Cheng D, Du Y, Guo X, Gao R, et al. RNF186 regulates EFNB1 (ephrin B1)-EPHB2-
789 induced autophagy in the colonic epithelial cells for the maintenance of intestinal homeostasis.
790 *Autophagy.* 2021;17(10):3030-47.

791 18. Vereecke L, Sze M, Mc Guire C, Rogiers B, Chu Y, Schmidt-Supprian M, et al. Enterocyte-specific
792 A20 deficiency sensitizes to tumor necrosis factor-induced toxicity and experimental colitis. *J*
793 *Exp Med.* 2010;207(7):1513-23.

19. Lin H, Feng L, Cui KS, Zeng LW, Gao D, Zhang LX, et al. The membrane-associated E3 ubiquitin ligase MARCH3 downregulates the IL-6 receptor and suppresses colitis-associated carcinogenesis. *Cell Mol Immunol.* 2021;18(12):2648-59.

20. Zou M, Zeng QS, Nie J, Yang JH, Luo ZY, and Gan HT. The Role of E3 Ubiquitin Ligases and Deubiquitinases in Inflammatory Bowel Disease: Friend or Foe? *Front Immunol.* 2021;12:769167.

21. Manning JA, and Kumar S. Physiological Functions of Nedd4-2: Lessons from Knockout Mouse Models. *Trends Biochem Sci.* 2018;43(8):635-47.

22. Goel P, Manning JA, and Kumar S. NEDD4-2 (NEDD4L): the ubiquitin ligase for multiple membrane proteins. *Gene.* 2015;557(1):1-10.

23. Verrey F, Fakitsas P, Adam G, and Staub O. Early transcriptional control of ENaC (de)ubiquitylation by aldosterone. *Kidney Int.* 2008;73(6):691-6.

24. Duerr J, Leitz DHW, Szczygiel M, Dvornikov D, Fraumann SG, Kreutz C, et al. Conditional deletion of Nedd4-2 in lung epithelial cells causes progressive pulmonary fibrosis in adult mice. *Nat Commun.* 2020;11(1):2012.

25. Henshall TL, Manning JA, Alfassy OS, Goel P, Boase NA, Kawabe H, et al. Deletion of Nedd4-2 results in progressive kidney disease in mice. *Cell Death Differ.* 2017;24(12):2150-60.

26. Gao S, Alarcon C, Sapkota G, Rahman S, Chen PY, Goerner N, et al. Ubiquitin ligase Nedd4L targets activated Smad2/3 to limit TGF-beta signaling. *Mol Cell.* 2009;36(3):457-68.

27. Novellasdemunt L, Kucharska A, Jamieson C, Prange-Barczynska M, Baulies A, Antas P, et al. NEDD4 and NEDD4L regulate Wnt signalling and intestinal stem cell priming by degrading LGR5 receptor. *EMBO J.* 2020;39(3):e102771.

816 28. Gao P, Ma X, Yuan M, Yi Y, Liu G, Wen M, et al. E3 ligase Nedd4l promotes antiviral innate
817 immunity by catalyzing K29-linked cysteine ubiquitination of TRAF3. *Nat Commun.*
818 2021;12(1):1194.
819 29. Li H, Wang N, Jiang Y, Wang H, Xin Z, An H, et al. E3 ubiquitin ligase NEDD4L negatively regulates
820 inflammation by promoting ubiquitination of MEKK2. *EMBO Rep.* 2022;23(11):e54603.
821 30. Liu H, Lin W, Liu Z, Song Y, Cheng H, An H, et al. E3 ubiquitin ligase NEDD4L negatively regulates
822 keratinocyte hyperplasia by promoting GP130 degradation. *EMBO Rep.* 2021;22(5):e52063.
823 31. Jiang C, Kawabe H, and Rotin D. The Ubiquitin Ligase Nedd4L Regulates the Na/K/2Cl Co-
824 transporter NKCC1/SLC12A2 in the Colon. *J Biol Chem.* 2017;292(8):3137-45.
825 32. Luo G, He Y, Yang F, Zhai Z, Han J, Xu W, et al. Blocking GSDME-mediated pyroptosis in renal
826 tubular epithelial cells alleviates disease activity in lupus mice. *Cell Death Discov.* 2022;8(1):113.
827 33. Tigano M, Vargas DC, Tremblay-Belzile S, Fu Y, and Sfeir A. Nuclear sensing of breaks in
828 mitochondrial DNA enhances immune surveillance. *Nature.* 2021;591(7850):477-81.
829 34. Wang Y, Gao W, Shi X, Ding J, Liu W, He H, et al. Chemotherapy drugs induce pyroptosis through
830 caspase-3 cleavage of a gasdermin. *Nature.* 2017;547(7661):99-103.
831 35. Xu D, Jin T, Zhu H, Chen H, Ofengeim D, Zou C, et al. TBK1 Suppresses RIPK1-Driven Apoptosis
832 and Inflammation during Development and in Aging. *Cell.* 2018;174(6):1477-91 e19.
833 36. Nguyen HT, Dalmasso G, Torkvist L, Halfvarson J, Yan Y, Laroui H, et al. CD98 expression
834 modulates intestinal homeostasis, inflammation, and colitis-associated cancer in mice. *J Clin*
835 *Invest.* 2011;121(5):1733-47.
836 37. Maspero E, Valentini E, Mari S, Cecatiello V, Soffientini P, Pasqualato S, et al. Structure of a
837 ubiquitin-loaded HECT ligase reveals the molecular basis for catalytic priming. *Nat Struct Mol*

Biol. 2013;20(6):696-701.

38. Brabec T, Voboril M, Schierova D, Valter E, Splichalova I, Dobes J, et al. IL-17-driven induction of Paneth cell antimicrobial functions protects the host from microbiota dysbiosis and inflammation in the ileum. *Mucosal Immunol.* 2023;16(4):373-85.

39. Chandra V, Li L, Le Roux O, Zhang Y, Howell RM, Rupani DN, et al. Gut epithelial Interleukin-17 receptor A signaling can modulate distant tumors growth through microbial regulation. *Cancer Cell.* 2024;42(1):85-100 e6.

40. Wang K, Kim MK, Di Caro G, Wong J, Shalapour S, Wan J, et al. Interleukin-17 receptor a signaling in transformed enterocytes promotes early colorectal tumorigenesis. *Immunity.* 2014;41(6):1052-63.

41. Yip KH, Kolesnikoff N, Hauschild N, Biggs L, Lopez AF, Galli SJ, et al. The Nedd4-2/Ndfip1 axis is a negative regulator of IgE-mediated mast cell activation. *Nat Commun.* 2016;7:13198.

42. Desai MS, Seekatz AM, Koropatkin NM, Kamada N, Hickey CA, Wolter M, et al. A Dietary Fiber-Deprived Gut Microbiota Degrades the Colonic Mucus Barrier and Enhances Pathogen Susceptibility. *Cell.* 2016;167(5):1339-53 e21.

43. Deng F, Zhao BC, Yang X, Lin ZB, Sun QS, Wang YF, et al. The gut microbiota metabolite capsiate promotes Gpx4 expression by activating TRPV1 to inhibit intestinal ischemia reperfusion-induced ferroptosis. *Gut Microbes.* 2021;13(1):1-21.

44. Tanaka T, Kohno H, Suzuki R, Yamada Y, Sugie S, and Mori H. A novel inflammation-related mouse colon carcinogenesis model induced by azoxymethane and dextran sodium sulfate. *Cancer Sci.* 2003;94(11):965-73.

45. Zaki MH, Vogel P, Malireddi RK, Body-Malapel M, Anand PK, Bertin J, et al. The NOD-like

receptor NLRP12 attenuates colon inflammation and tumorigenesis. *Cancer Cell.* 2011;20(5):649-60.

46. Yang Y, Huycke MM, Herman TS, and Wang X. Glutathione S-transferase alpha 4 induction by activator protein 1 in colorectal cancer. *Oncogene.* 2016;35(44):5795-806.

47. Wang X, Yang Y, and Huycke MM. Commensal bacteria drive endogenous transformation and tumour stem cell marker expression through a bystander effect. *Gut.* 2015;64(3):459-68.

48. Gobert AP, Boutaud O, Asim M, Zagol-Ikapitte IA, Delgado AG, Latour YL, et al. Dicarbonyl Electrophiles Mediate Inflammation-Induced Gastrointestinal Carcinogenesis. *Gastroenterology.* 2021;160(4):1256-68 e9.

49. Chen Y, Zhang P, Chen W, and Chen G. Ferroptosis mediated DSS-induced ulcerative colitis associated with Nrf2/HO-1 signaling pathway. *Immunol Lett.* 2020;225:9-15.

50. Wang S, Liu W, Wang J, and Bai X. Curculigoside inhibits ferroptosis in ulcerative colitis through the induction of GPX4. *Life Sci.* 2020;259:118356.

51. Guarnieri AL, Towers CG, Drasin DJ, Oliphant MUJ, Andrysik Z, Hotz TJ, et al. The miR-106b-25 cluster mediates breast tumor initiation through activation of NOTCH1 via direct repression of NEDD4L. *Oncogene.* 2018;37(28):3879-93.

52. Li G, Song Z, Wu C, Li X, Zhao L, Tong B, et al. Downregulation of NEDD4L by EGFR signaling promotes the development of lung adenocarcinoma. *J Transl Med.* 2022;20(1):47.

53. Kalliolias GD, and Ivashkiv LB. TNF biology, pathogenic mechanisms and emerging therapeutic strategies. *Nat Rev Rheumatol.* 2016;12(1):49-62.

54. Popovic D, Vucic D, and Dikic I. Ubiquitination in disease pathogenesis and treatment. *Nat Med.* 2014;20(11):1242-53.

882 55. Cockram PE, Kist M, Prakash S, Chen SH, Wertz IE, and Vucic D. Ubiquitination in the regulation
883 of inflammatory cell death and cancer. *Cell Death Differ.* 2021;28(2):591-605.
884 56. Liu J, Qian C, and Cao X. Post-Translational Modification Control of Innate Immunity. *Immunity.*
885 2016;45(1):15-30.
886 57. Fiore A, Zeitler L, Russier M, Gross A, Hiller MK, Parker JL, et al. Kynurenine importation by
887 SLC7A11 propagates anti-ferroptotic signaling. *Mol Cell.* 2022;82(5):920-32 e7.
888 58. Cao T, Zhou J, Liu Q, Mao T, Chen B, Wu Q, et al. Interferon-gamma induces salivary gland
889 epithelial cell ferroptosis in Sjogren's syndrome via JAK/STAT1-mediated inhibition of system
890 Xc(). *Free Radic Biol Med.* 2023;205:116-28.
891 59. Brennan CA, and Garrett WS. Gut Microbiota, Inflammation, and Colorectal Cancer. *Annu Rev*
892 *Microbiol.* 2016;70:395-411.
893 60. Lu C, Thoeni C, Connor A, Kawabe H, Gallinger S, and Rotin D. Intestinal knockout of Nedd4
894 enhances growth of Apc(min) tumors. *Oncogene.* 2016;35(45):5839-49.
895 61. Chuang HY, Hsu LY, Pan CM, Pikatan NW, Yadav VK, Fong IH, et al. The E3 Ubiquitin Ligase
896 NEDD4-1 Mediates Temozolomide-Resistant Glioblastoma through PTEN Attenuation and
897 Redox Imbalance in Nrf2-HO-1 Axis. *Int J Mol Sci.* 2021;22(19).
898 62. Hong Z, Cao J, Liu D, Liu M, Chen M, Zeng F, et al. Celastrol targeting Nedd4 reduces Nrf2-
899 mediated oxidative stress in astrocytes after ischemic stroke. *J Pharm Anal.* 2023;13(2):156-69.
900 63. Wu J, Minikes AM, Gao M, Bian H, Li Y, Stockwell BR, et al. Intercellular interaction dictates
901 cancer cell ferroptosis via NF2-YAP signalling. *Nature.* 2019;572(7769):402-6.
902 64. Wei Y, Yee PP, Liu Z, Zhang L, Guo H, Zheng H, et al. NEDD4L-mediated Merlin ubiquitination
903 facilitates Hippo pathway activation. *EMBO Rep.* 2020;21(12):e50642.

65. Lin W, Ma C, Su F, Jiang Y, Lai R, Zhang T, et al. Raf kinase inhibitor protein mediates intestinal epithelial cell apoptosis and promotes IBDs in humans and mice. *Gut.* 2017;66(4):597-610.

Figure legends

Figure 1. NEDD4L Expression is significantly down-regulated in intestinal epithelial cells (IECs) of patients with IBDs.

(A, B) Statistical analysis of NEDD4L immunohistochemical (IHC) intensity in the biopsies from Xijing Hospital (cohort1) **(A)** and representative IHC staining of sections traced with anti-NEDD4L antibody **(B)**. Normal control (HC) n=40 and UC n=83. Scale bar, 50 μm. **(C, D)** Statistical analysis of NEDD4L IHC intensity in the biopsies from the First Affiliated Hospital of Zhejiang University, School of Medicine (FAHZU, cohort2) **(C)** and representative IHC staining of sections **(D)**. Normal control (HC) n=31, UC n=36, and CD n=41. Scale bar, 50 μm. **(E, F)** Statistical analysis of NEDD4L IHC intensity in the biopsies with disease status record from cohort 2 and representative IHC staining of sections traced with anti-NEDD4L antibody**(F)**. Mild n=14 and Moderate/Severe n=48. Scale bar, 50 μm. **(G, H)** qPCR analysis **(G)** and representative western blotting of NEDD4L in the mucosa from patients with IBDs and their corresponding normal tissues (n=24/group). **(I, J)** Western blotting analysis **(I)** and protein intensity analysis **(J)** according to **(I)** using ImageJ software of NEDD4L form the IECs of the wild-type (WT) mice treated without or with DSS for 4 days (n=5/group). Red arrows indicated NEDD4L expression in IECs, and green arrows indicated NEDD4L expression in non-IECs.

Data represent mean ± SEM. Each dot means independent samples. ns, no significant difference. ****, P<0.0001; ***, P<0.001; **, P<0.01. Statistical analysis was performed using 1-way ANOVA multiple comparisons in **C,** and a 2-tailed Student's t-test in **A, E, G,** and **J**.

Figure 2. *Nedd4l* deficiency in mice promotes dextran sulfate sodium (DSS)-induced experimental colitis in a non-hematopoietic cell-dependent manner.

(A) *Nedd4l* global-deficient mice (*Nedd4l*$^{+/-}$) and control littermates (*Nedd4l*$^{+/+}$) were administered with 4 % DSS for 5 days followed by water to induce acute colitis. Mouse death was monitored until day 9. n=20/group. **(B-D)** *Nedd4l*$^{+/-}$ mice and *Nedd4l*$^{+/+}$ were administered with 3 % DSS for 5 days followed by water until day 9. n=9/group. **(B)**Body weight change, **(C)** bleeding scores, **(D)** colon length, **(E)** gross morphology images, and

(F) H&E staining of the colons from *Nedd4l*$^{+/+}$ and *Nedd4l*$^{+/-}$mice. Red arrows point to epithelial degeneration and green arrows to inflammatory infiltrates. Scale bar, 200 μm or 50 μm (amplified sections). **(G–J)** The bone marrow from *Nedd4l*$^{+/+}$(WT) and *Nedd4l*$^{-/-}$ (KO) mice were transferred to WT (n=7) and KO(n=10) mice to generate bone marrow reconstitution mice. The bone marrow reconstitution mice were subjected to 3% DSS treatment for 5 days followed by water, and **(G)** mouse death and **(H)** body weight changes were monitored until day 9. **(I, J)** In a separate experiment, **(I)**colon length and **(J)** gross morphology images of the colons from mice on day 6 after DSS treatment. n=4/group. Red arrows point to epithelial degeneration and green arrows to inflammatory infiltrates.

Data represent mean ± SEM from at least two independent experiments. Each dot means independent samples. ns, no significant difference. ****, P<0.0001; ***, P<0.001; **, P<0.01. Statistical analysis was performed using a log-rank test in **A** and **G**, a two-way ANOVA test in **B**, **C**, and **H**, and a 2-tailed Student's t-test in **D** and **I**.

Figure 3. *Nedd4l* deficiency in IECs promotes DSS-induced colitis in mice.

(A) *Nedd4l* IEC-deficient mice (*Nedd4l*$^{f/f}$*Villin*^{Cre}, n=8) and control littermates (*Nedd4l*$^{f/f}$, n=7) were administered with 2.5 % DSS for 5 days followed by water to induce acute colitis. Mouse death was monitored until day 12. **(B-F)** In a separate experiment, *Nedd4l*$^{f/f}$*Villin*^{Cre} (n=7) mice and control *Nedd4l*$^{f/f}$ (n=8) mice were administered with 2% DSS for 5 days followed by water until day 9 to induce colitis. **(B)** Body weight change, **(C)** bleeding scores, **(D)** colon length, **(E)** gross morphology images, and **(F)** H&E staining of the colons from *Nedd4l*$^{f/f}$*Villin*^{Cre} and *Nedd4l*$^{f/f}$ mice. Red arrows point to epithelial degeneration and green arrows to inflammatory infiltrates. Scale bar, 200 μm or 50 μm (amplified sections). **(G, H)** Colon-infiltrated immune cells of *Nedd4l*$^{f/f}$*Villin*^{Cre} and *Nedd4l*$^{f/f}$ mice from **(B)** were analyzed by flow cytometer analysis (n = 3–4/group). Red arrows point to epithelial degeneration and green arrows to inflammatory infiltrates.

Data represent mean ± SEM from at least two independent experiments. Each dot means independent samples. ns, no significant difference. ***, P<0.001; **, P<0.01; *, P<0.05. Statistical analysis was performed using a log-rank test in **A**, a two-way ANOVA test in **B** and **C**, and a 2-tailed Student's t-test in **D**, **G**, and **H**.

Figure 4. *Nedd4l* deficiency in IECs promotes IEC ferroptosis, resulting in barrier integrity damage.

(A) KEGG analysis of colonic tissues on the 7th day from the *Nedd4l*$^{f/f}$*Villin*^{Cre} and *Nedd4l*$^{f/f}$ mice administered 2 % DSS. **(B)** The indicated mice were treated as in **(A)** and were orally fed with FITC-dextran (500 mg/kg) for 4 h before sacrifice. The serum levels of FITC-dextran were detected by measuring the mean fluorescence intensity (MFI) of FITC-dextran. **(C)** In a separate experiment, the indicated mice were treated as in **(A)**, and colon tissues were further subjected to ZO-1 immunofluorescence (IF) staining. Red IF indicated ZO-1 and blue (DAPI) indicated nucleic. Scale bars, 50 μm. **(D)** KEGG analysis of ubiquitylation mass spectrometry from IECs of the indicated mice treated as in **(A)**. **(E-H)** Colon tissues from DSS-treated *Nedd4l*$^{f/f}$*Villin*^{Cre} and *Nedd4l*$^{f/f}$ mice were subjected to TUNEL **(E, F)** and 4-HNE **(G, H)** IHC staining. The TUNEL **(F)** and 4-HNE **(H)** IHC staining were scored and analyzed. Scale bars, 50 μm. **(I)** In a separate experiment, the IECs from DSS-treated *Nedd4l*$^{f/f}$*Villin*^{Cre} and *Nedd4l*$^{f/f}$ mice were subjected to MDA analysis. **(J)** Representative transmission electron microscope (TEM) images from colonic tissue sections of DSS-treated *Nedd4l*$^{f/f}$*Villin*^{Cre} and *Nedd4l*$^{f/f}$ mice. Scale bars, 2μm or 0.5 μm (amplified sections). **(K, L)** Representative microscope images **(K)** and flow cytometer analysis **(L)** of small intestinal organoids isolated and cultured from crypts of *Nedd4l*$^{f/f}$*Villin*^{Cre} and *Nedd4l*$^{f/f}$ mice treated with DMSO(Control), DSS (0.5% w/v), Erastin(30μM), Erastin2 (30μM), and RSL3 (5μM) for 24hr, followed by DAPI and BODIPY C11 staining. n = 3/group. Scale bars, 100 μm.

Data represent mean ± SEM from at least two independent experiments. Each dot means independent samples. ns, no significant difference. *P<0.05, **P<0.01. Statistical analysis was performed using a 2-tailed Student's t-test in **B**, **E**, **H**, **I**, and **L**.

Figure 5. NEDD4L positively regulates SLC3A2 expression.

(A) Volcano plots of protein abundance fold change based on ubiquitylation mass spectrometry of **Figure 4D**. **(B)** Venn analysis showed the potential targets of NEDD4L based on interaction MS analysis in Flag-tagged NEDD4L stable expressed HCT116 cells and ubiquitylation MS analysis. The list showed the overlapped targets of NEDD4L in **(A)**

and **(B)**. **(C)** Representative IHC staining of SLC3A2 from *Nedd4l*$^{f/f}$*Villin*^{Cre} and *Nedd4l*$^{f/f}$ mice treated with DSS on day 5. Scale bar, 100 μm or 50 μm (amplified sections). **(D, E)** Western blotting analysis **(D)** and statistical analysis **(E)** of the indicated protein intensity in the IECs from *Nedd4l*$^{f/f}$*Villin*^{Cre} (n =7) and *Nedd4l*$^{f/f}$ (n =4) mice treated as **Figure 3B. (F, G)** Representative IHC staining **(F)** and correlative analysis **(G)** of SLC3A2 and NEDD4L from colonic sections from CD patients (n=13). Scale bars, 50 μm. **(H)** Immunoblot analysis of the indicated proteins in small intestinal organoids isolated and cultured from crypts of *Nedd4l*$^{f/f}$*Villin*^{Cre} and *Nedd4l*$^{f/f}$ mice, with 0.5% DSS treatment for the indicated time. **(I, J)** *NEDD4L* knockout (sg*NEDD4L*) and negative control(sg*NTC*) HCT116 cell lines, or Myc-tagged NEDD4L, Myc-tagged NEDD4L-C942A(Myc-NEDD4L-CA), or Myc-tagged null control plasmids (Ctrl) transfected HCT116 cells were treated with 2% DSS for the indicated time and then subjected to immunoblot analysis of the indicated proteins. **(K-M)** Immunoblot analysis of the indicated proteins in HCT116 cells **(K)**, SW480 cells **(L)**, and RKO cells **(M)** transfected with the siRNA targeted to NEDD4L (si*NEDD4L*) or negative control (si*NC*) and treated as in**(I)**.

Data represent mean ± SEM from at least two independent experiments. Each dot means independent samples. ns, no significant difference. ***, P<0.001; **, P<0.01; *, P<0.05. Statistical analysis was performed using a 2-tailed Student's t-test in **E**, and a Pearson correlation test in **G**.

Figure 6. SLC3A2 negatively regulates ferroptosis.

(A-C) The multitype cell lines, including HCT116 cells **(A)**, SW480 cells **(B)**, and RKO cells **(C)** were transfected with the siRNA targeted to *SLC3A2* (si*SLC3A2*) or negative control (si*NC*). The cells were treated with 2% DSS for the indicated time and then subjected to CCK8 assay. **(D-F)** The multitype cell lines were treated as in **(A-C)** with or without Fer-1(2μM) treatment. The cells were then subjected to flow cytometer analysis of BODIPY C11 staining to measure lipid peroxidation production. **(G-I)** The multitype cell lines were treated as in **(A-C)** for the indicated time and then subjected to immunoblot analysis of the indicated proteins. **(J-M)** HCT116 cells were overexpressed with Flag-tagged SLC3A2 or Flag-tagged null control plasmids. The cells were treated with 2% DSS or indicated

inducers for the stated time, and then subjected to CCK8 assay **(J)**, MDA assay**(K)**, flow cytometer analysis of BODIPY C11 staining **(L)**, and immunoblot analysis of immunoblot analysis of the indicated proteins **(M)**. **(N-P)** HCT116 cells were transfected with siRNA negative control (si*NC*) or NEDD4L (si*NEDD4L*) specific oligo and then overexpressed with Flag-tagged SLC3A2 or Flag-tagged null control plasmid. The cells were treated with 2% DSS for the indicated time and then subjected to CCK8 assay**(N)** and lipid peroxidation **(O)**. Immunoblot analysis of the indicated proteins **(P).**

Data represent mean ± SEM from at least two independent experiments. Each dot means independent samples. ns, no significant difference. ***, P<0.001; **, P<0.01; *, P<0.05. Statistical analysis was performed using a 2-tailed Student's t-test in **A-F**, **J-K**, **N**, and **O.**

Figure 7. NEDD4L ubiquitinates SLC3A2.

(A) Immunoblot analysis of NEDD4L and SLC3A2 co-immunoprecipitated with anti-SLC3A2 antibody from lysates of HCT116 cells treated with 2%DSS for the indicated time. **(B, C)** Immunoblot analysis of Myc-tagged proteins and Flag-tagged SLC3A2 co-immunoprecipitated with anti-Myc antibody from lysates of HEK293T cells co-transfected with indicated plasmids. **(D)** Immunoblot analysis of NEDD4L, SLC3A2, and Ub, which were co-immunoprecipitated with anti-Ub antibody from lysates of NEDD4L (sg*NEDD4L*) or negative control (sg*NTC*) knockout HCT116 cells treated with 2%DSS for the indicated time. **(E)** Immunoblot analysis of total ubiquitination of Flag-tagged SLC3A2 following co-immunoprecipitated of Flag-tagged with anti-Flag antibody from lysates of HEK293T cells co-transfected with indicated plasmids. **(F)** Immunoblot analysis of Ub-linked flag-tagged EGFP or SLC3A2 incubated with Myc-tagged NEDD4L, Myc-tagged NEDD4L-C942A (CA), or Myc-tagged EGFP recombinant protein in the present of the full complement of ubiquitination reaction components, including E1, E2, Ub, and ATP in vitro. **(G, H)** Immunoblot analysis of ubiquitination of Flag-tagged SLC3A2 following co-immunoprecipitated of SLC3A2 with anti-Flag antibody from lysates of HEK293T cells co-transfected with indicated plasmids. **(I)** Immunoblot analysis of K63Ub, K48Ub, Ub, GPX4, TFRC, SLC3A2, NEDD4L, and actin, which was co-immunoprecipitated with anti-SLC3A2 antibody from lysates of NEDD4L (sg*NEDD4L*) or negative control (sg*NTC*) knockout

HCT116 cells treated with 2%DSS for the indicated time pre-treated with 20μM MG-132 for 6 hr. **(J)** Immunoblot analysis of total ubiquitination of Flag-tagged SLC3A2 following co-immunoprecipitating of SLC3A2 with anti-Flag antibody from lysates of HEK293T cells co-transfected with indicated plasmids.

Figure 8. NEDD4L regulates DSS-induced colitis through ferroptosis.

Nedd4l$^{f/f}$*Villin*^{Cre} and *Nedd4l*$^{f/f}$ mice pre-treated with ferrostatin-1 (Fer1, 5μM/Kg) or DMSO were administered with 2% DSS for 5 days, and on the 9th day the mice were sacrificed for collecting colonic tissues and IECs. *Nedd4l*$^{f/f}$+DMSO n=3, *Nedd4l*$^{f/f}$*Villin*^{Cre}+DMSO n=4, *Nedd4l*$^{f/f}$+Fer-1 n=6, *Nedd4l*$^{f/f}$*Villin*^{Cre}+Fer-1 n=4. **(A)** Body weight change, **(B)** colon length, **(C)** gross morphology images, **(D)** histological score, **(E)** representative H&E staining, and **(F)** TUNEL staining of the colon sections from the indicated mice. **(G-J)** In a separate experiment, the IECs and colon tissues from mice treated as in **(A)** were subjected to flow cytometer analysis of EpCAM, CD45, and PI staining **(G, H),** 4-HNE IHC staining **(I),** and ZO-1 IF staining **(J)**. **(K)** qPCR analysis, **(L)** western blotting analysis, and **(M)** protein intensity analysis of the indicated proteins of IECs treated as in**(A)**. *Nedd4l*$^{f/f}$+DMSO n=3-5, *Nedd4l*$^{f/f}$*Villin*^{Cre}+DMSO n=3, *Nedd4l*$^{f/f}$ +Fer-1 n=4-6, *Nedd4l*$^{f/f}$*Villin*^{Cre}+Fer-1 n=3-5, as indicated in the figure. Scale bar, 50 μm.

Data represent mean ± SEM from at least two independent experiments. Each dot means independent samples. ns, no significant difference. *P<0.05, **P<0.01. Statistical analysis was performed using a two-way ANOVA test in **A**, 1-way ANOVA multiple comparisons **B**, **D**, **G**, **H**, **K**, and **M**.

Figure 9. *Nedd4l* deficiency in IECs promotes AOM/DSS-induced colorectal cancer in mice.

(A) MRI images of *Nedd4l*$^{f/f}$*Villin*^{Cre} and *Nedd4l*$^{f/f}$ mice treated with AOM/DSS for 90 days. **(B-D)** Tumor numbers (*Nedd4l*$^{f/f}$ n=15, *Nedd4l*$^{f/f}$*Villin*^{Cre} n=21) **(B)**, tumor size (n=6/group) **(C)**, and representative morphology images of colons **(D)** from the AOM/DSS-treated mice on day 90. **(E-G)** Representative IHC staining of sections from the tumor, adjacent tumor, and distal normal tissues of AOM/DSS-treated *Nedd4l*$^{f/f}$*Villin*^{Cre} and *Nedd4l*$^{f/f}$ mice with anti-Ki67antibody **(E)**, anti-4-HNE antibody **(F)**, and **(G)**statistical analysis of Ki67 positive cells

according to (n=4/group) **(E)**. **(H-L)** Schematic diagram of the treatment plan for AOM/DSS-treated *Nedd4l*$^{f/f}$*Villin*^{Cre} and *Nedd4l*$^{f/f}$ mice with ddH_2O or DFOM**(H)**. Representative morphology images of colons **(I)**, tumor numbers**(J)**, statistical analysis of 4-HNE IHC staining score **(K)**, and representative images of 4-HNE IHC staining from the treated mice as in **(I)**. *Nedd4l*$^{f/f}$+ddH_2O n=5, *Nedd4l*$^{f/f}$*Villin*^{Cre}+ddH_2O n=5, *Nedd4l*$^{f/f}$+DFOM n=8, *Nedd4l*$^{f/f}$*Villin*^{Cre}+DFOM n=8. Scale bars, 50 μm.

Data represent mean ± SEM from at least two independent experiments. Each dot means independent samples. ns, no significant difference. ***, P<0.001; **, P<0.01; *, P<0.05. Statistical analysis was performed using a 2-tailed Student's t-test in **B**, **C**, and **F**, and 1-way ANOVA multiple comparisons in **J**, and **K**.

Figure 10. Expression of NEDD4L is significantly down-regulated in IECs of patients and mice with colorectal cancer.

(A-D) Wild-type mice were treated with AOM/DSS, and the IECs (on day 0, day 15, and day 60) and tumor nods (on day 90) were collected for immunoblot analysis **(A),** protein intensity analysis**(B)**, qPCR analysis **(C)**, and **(D)** correlative analysis of the indicated proteins. n=3/group. **(E, F)** Representative NEDD4L and 4-HNE IHC staining of sections from the tumor, adjacent tumor, and distal normal tissues of patients with colorectal cancer **(E)**, and statistical analysis of NEDD4L and 4-HNE IHC staining intensity **(F)** according to **(E)**. (n=55) **(G, H)**. Representative SLC3A2, GPX4, and NEDD4L IHC staining sections from the tumor tissues of patients with colorectal cancer **(G)**, and correlative analysis between SLC3A2, GPX4, and NEDD4L IHC staining intensity score (n=55) **(H)**. Scale bars, 50 μm.

Data represent mean ± SEM from at least two independent experiments. Each dot means independent samples. ns, no significant difference. ***, P<0.001; **, P<0.01; *, P<0.05. Statistical analysis was performed using 1-way ANOVA multiple comparisons in **B**, **C**, and **F**, and a Pearson correlation test in **D** and **H**.

Table1 NEDD4L expression in patients with UC from Xijing Hospital

NEDD4L					
Group types	Total No. studied	NEDD4L			
		-	+	++	+++
		%	%	%	%
Normal	40	4(10%)	2(5%)	26(65%)	8(20%)
Ulcerative colitis	83***	32(38.5%)	10(12.1%)	37(44.6%)	4(4.8%)

Note: Correlations were analyzed using Pearson's χ^2 test.

***P<0.001 compared with normal tissues.

Table2 NEDD4L expression in patients with UC and CD from FAHZU Hospital

NEDD4L					
Group types	Total No. studied	NEDD4L			
		-	+	++	+++
		%	%	%	%
Normal	31	0(0%)	0(0%)	1(3.2%)	30(96.8%)
Ulcerative colitis	36***	1(2.8%)	2(5.6%)	19(52.8%)	14(38.8%)
Crohn's disease	41***	0(0%)	1(2.4%)	24(58.6%)	16(39%)

Note: Correlations were analyzed using Pearson's χ^2 test.

***P<0.001 compared with normal tissues.

Figure 1

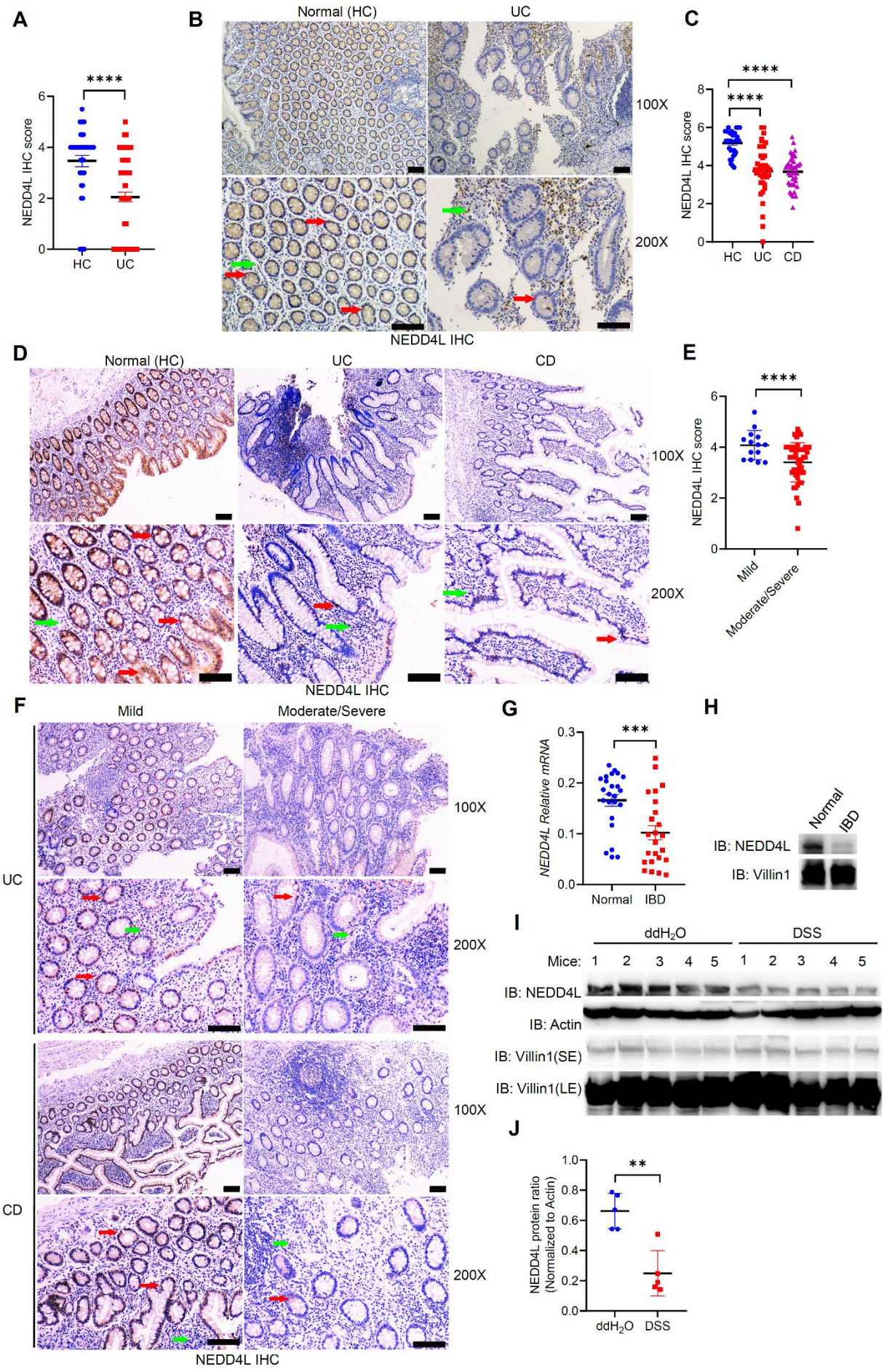
A
NEDD4L IHC score
HC
UC
****
B
Normal (HC)
UC
100X
200X
NEDD4L IHC
C
NEDD4L IHC score
HC
UC
CD
****
D
Normal (HC)
UC
CD
100X
200X
NEDD4L IHC
E
NEDD4L IHC score
Mild
Moderate/Severe
F
Mild
Moderate/Severe
UC
CD
100X
200X
NEDD4L IHC
G
NEDD4L Relative mRNA
Normal
IBD
H
Normal
IBD
IB: NEDD4L
IB: Villin1
I
ddH2O
DSS
Mice: 1 2 3 4 5 1 2 3 4 5
IB: NEDD4L
IB: Actin
IB: Villin1(SE)
IB: Villin1(LE)
J
NEDD4L protein ratio (Normalized to Actin)
ddH2O
DSS

Figure 2

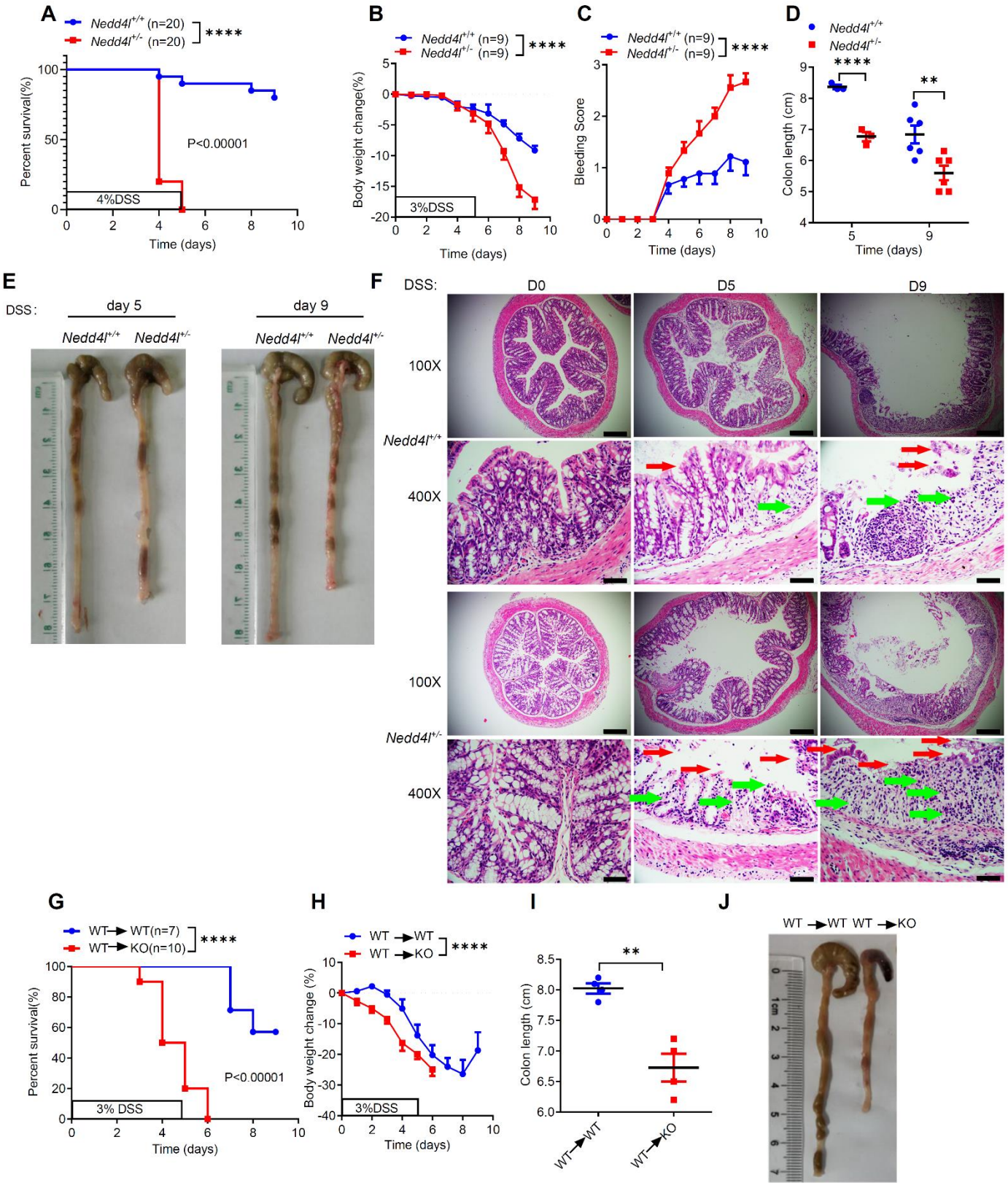
A
Nedd4l+/+ (n=20)
Nedd4l+/- (n=20)
****
Percent survival(%)
P<0.00001
4%DSS
Time (days)
B
Nedd4l+/+ (n=9)
Nedd4l+/- (n=9)
****
Body weight change(%)
3%DSS
Time (days)
C
Nedd4l+/+ (n=9)
Nedd4l+/- (n=9)
****
Bleeding Score
Time (days)
D
Nedd4l+/+
Nedd4l+/-
****
**
Colon length (cm)
Time (days)
E
DSS:
day 5
day 9
Nedd4l+/+
Nedd4l+/-
F
DSS:
D0
D5
D9
100X
Nedd4l+/+
400X
100X
Nedd4l+/-
400X
G
WT→WT(n=7)
WT→KO(n=10)
****
Percent survival(%)
P<0.00001
3% DSS
Time (days)
H
WT →WT
WT →KO
****
Body weight change (%)
3%DSS
Time (days)
I
**
Colon length (cm)
WT→WT
WT→KO
J
WT →WT WT →KO

Figure 3

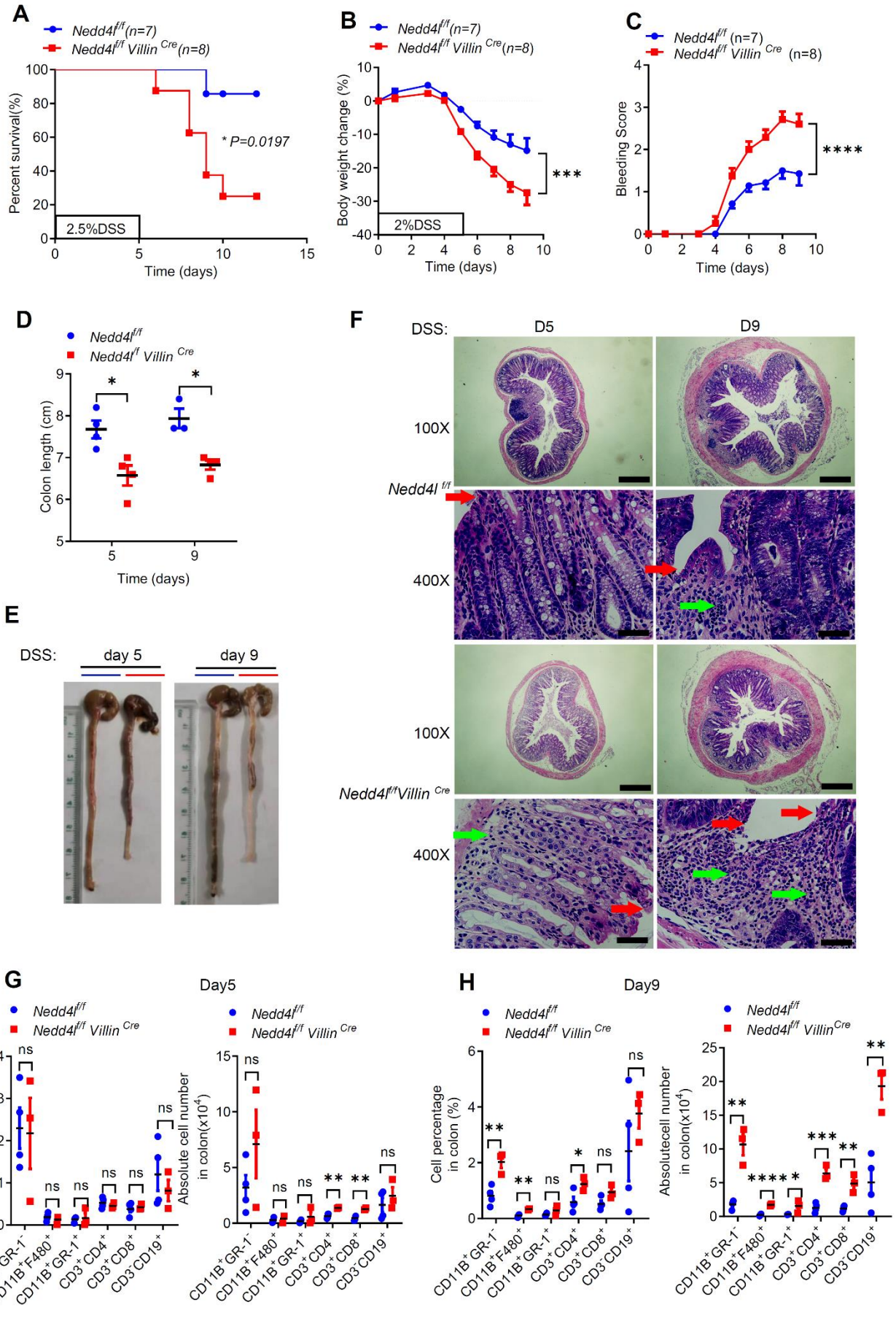
A
Nedd4l f/f (n=7)
Nedd4l f/f Villin Cre (n=8)
Percent survival(%)
* P=0.0197
2.5%DSS
Time (days)
B
Nedd4l f/f (n=7)
Nedd4l f/f Villin Cre (n=8)
Body weight change (%)
***
2%DSS
Time (days)
C
Nedd4l f/f (n=7)
Nedd4l f/f Villin Cre (n=8)
Bleeding Score
****
Time (days)
D
Nedd4l f/f
Nedd4l f/f Villin Cre
Colon length (cm)
Time (days)
E
DSS:
day 5
day 9
F
DSS:
D5
D9
100X
Nedd4l f/f
400X
100X
Nedd4l f/f Villin Cre
400X
G
Day5
Nedd4l f/f
Nedd4l f/f Villin Cre
Cell percentage in colon (%)
Absolute cell number in colon(x10^4)
CD11B+GR-1-
CD11B+F480+
CD11B+GR-1+
CD3+CD4+
CD3+CD8+
CD3-CD19+
H
Day9
Nedd4l f/f
Nedd4l f/f Villin Cre
Cell percentage in colon (%)
Absolutecell number in colon(x10^4)

Figure 4

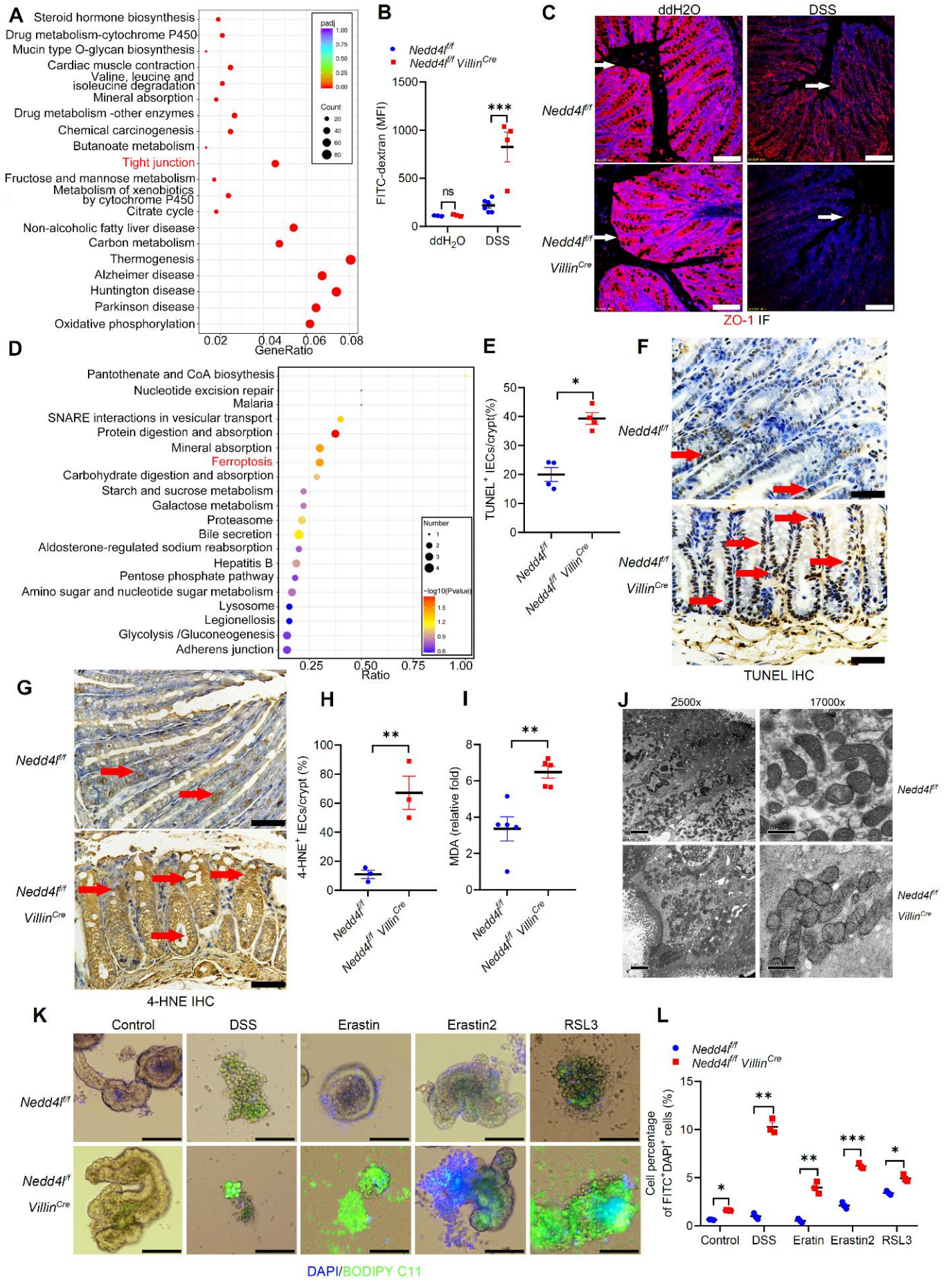
A
Steroid hormone biosynthesis
Drug metabolism-cytochrome P450
Mucin type O-glycan biosynthesis
Cardiac muscle contraction
Valine, leucine and isoleucine degradation
Mineral absorption
Drug metabolism -other enzymes
Chemical carcinogenesis
Butanoate metabolism
Tight junction
Fructose and mannose metabolism
Metabolism of xenobiotics by cytochrome P450
Citrate cycle
Non-alcoholic fatty liver disease
Carbon metabolism
Thermogenesis
Alzheimer disease
Huntington disease
Parkinson disease
Oxidative phosphorylation
padj
Count
GeneRatio
B
Nedd4lf/f
Nedd4lf/f VillinCre
FITC-dextran (MFI)
ns
***
ddH2O
DSS
C
ddH2O
DSS
Nedd4lf/f
Nedd4lf/f VillinCre
ZO-1 IF
D
Pantothenate and CoA biosythesis
Nucleotide excision repair
Malaria
SNARE interactions in vesicular transport
Protein digestion and absorption
Mineral absorption
Ferroptosis
Carbohydrate digestion and absorption
Starch and sucrose metabolism
Galactose metabolism
Proteasome
Bile secretion
Aldosterone-regulated sodium reabsorption
Hepatitis B
Pentose phosphate pathway
Amino sugar and nucleotide sugar metabolism
Lysosome
Legionellosis
Glycolysis /Gluconeogenesis
Adherens junction
Number
-log10(Pvalue)
Ratio
E
TUNEL+ IECs/crypt(%)
*
Nedd4lf/f
Nedd4lf/f VillinCre
F
Nedd4lf/f
Nedd4lf/f VillinCre
TUNEL IHC
G
Nedd4lf/f
Nedd4lf/f VillinCre
4-HNE IHC
H
4-HNE+ IECs/crypt (%)
**
Nedd4lf/f
Nedd4lf/f VillinCre
I
MDA (relative fold)
**
Nedd4lf/f
Nedd4lf/f VillinCre
J
2500x
17000x
Nedd4lf/f
Nedd4lf/f VillinCre
K
Control
DSS
Erastin
Erastin2
RSL3
Nedd4lf/f
Nedd4lf/f VillinCre
DAPI/BODIPY C11
L
Nedd4lf/f
Nedd4lf/f VillinCre
Cell percentage of FITC+DAPI+ cells (%)
Control
DSS
Eratin
Erastin2
RSL3

Figure 5

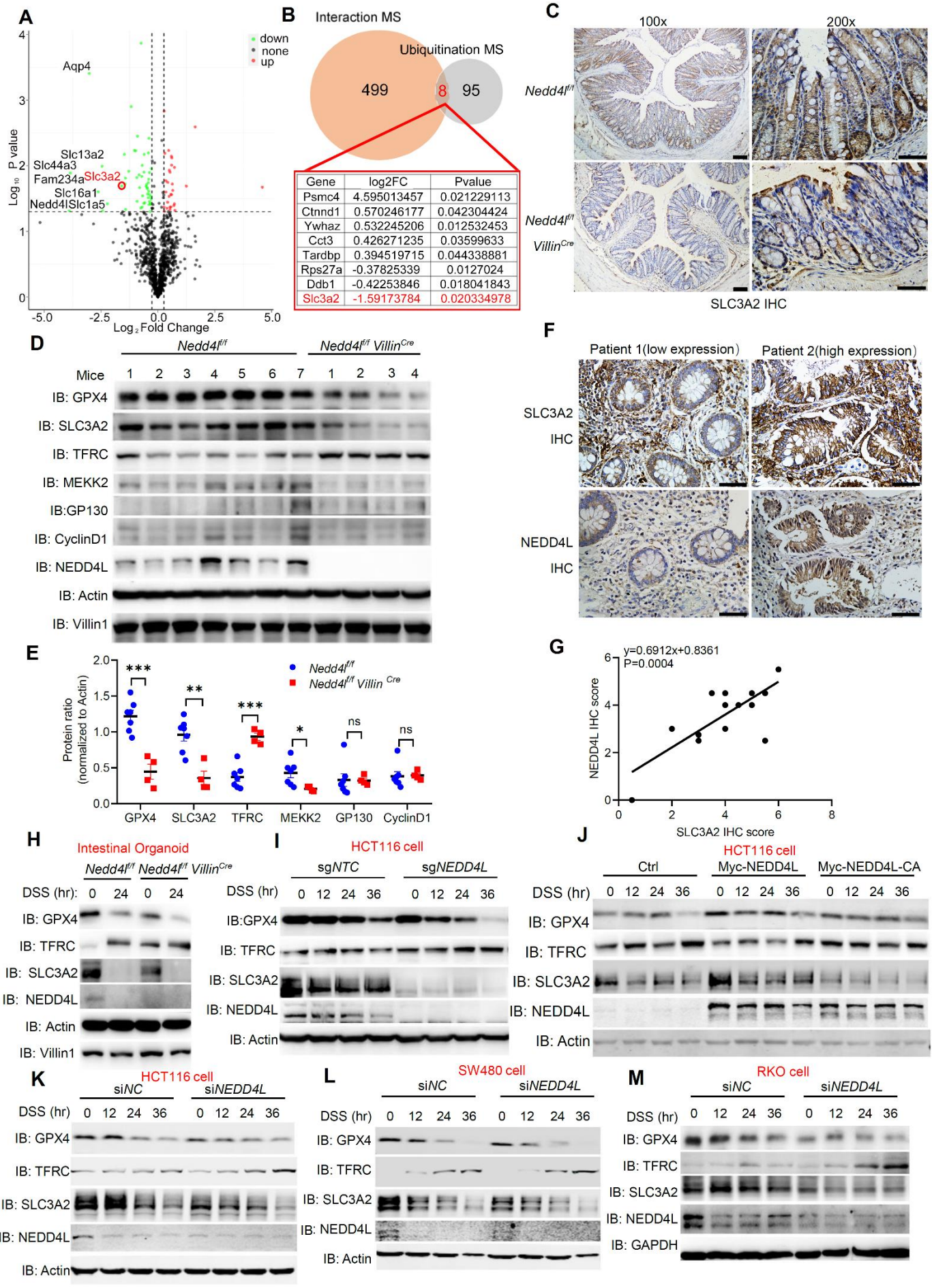
A
down
none
up
Aqp4
Slc13a2
Slc44a3
Fam234a
Slc3a2
Slc16a1
Nedd4l
Slc1a5
P value
Log2 Fold Change
B
Interaction MS
Ubiquitination MS
499
8
95
Gene | log2FC | Pvalue
Psmc4 | 4.595013457 | 0.021229113
Ctnnd1 | 0.570246177 | 0.042304424
Ywhaz | 0.532245206 | 0.012532453
Cct3 | 0.426271235 | 0.03599633
Tardbp | 0.394519715 | 0.044338881
Rps27a | -0.37825339 | 0.0127024
Ddb1 | -0.42253846 | 0.018041843
Slc3a2 | -1.59173784 | 0.020334978
C
100x
200x
Nedd4lf/f
Nedd4lf/f Villincre
SLC3A2 IHC
D
Nedd4lf/f
Nedd4lf/f Villincre
Mice 1 2 3 4 5 6 7 1 2 3 4
IB: GPX4
IB: SLC3A2
IB: TFRC
IB: MEKK2
IB:GP130
IB: CyclinD1
IB: NEDD4L
IB: Actin
IB: Villin1
E
Nedd4lf/f
Nedd4lf/f Villin Cre
Protein ratio (normalized to Actin)
GPX4
SLC3A2
TFRC
MEKK2
GP130
CyclinD1
F
Patient 1(low expression)
Patient 2(high expression)
SLC3A2 IHC
NEDD4L IHC
G
y=0.6912x+0.8361
P=0.0004
NEDD4L IHC score
SLC3A2 IHC score
H
Intestinal Organoid
Nedd4lf/f
Nedd4lf/f Villincre
DSS (hr): 0 24 0 24
IB: GPX4
IB: TFRC
IB: SLC3A2
IB: NEDD4L
IB: Actin
IB: Villin1
I
HCT116 cell
sgNTC
sgNEDD4L
DSS (hr) 0 12 24 36 0 12 24 36
IB:GPX4
IB: TFRC
IB: SLC3A2
IB: NEDD4L
IB: Actin
J
HCT116 cell
Ctrl
Myc-NEDD4L
Myc-NEDD4L-CA
DSS (hr) 0 12 24 36 0 12 24 36 0 12 24 36
IB: GPX4
IB: TFRC
IB: SLC3A2
IB: NEDD4L
IB: Actin
K
HCT116 cell
siNC
siNEDD4L
DSS (hr) 0 12 24 36 0 12 24 36
IB: GPX4
IB: TFRC
IB: SLC3A2
IB: NEDD4L
IB: Actin
L
SW480 cell
siNC
siNEDD4L
DSS (hr) 0 12 24 36 0 12 24 36
IB: GPX4
IB: TFRC
IB: SLC3A2
IB: NEDD4L
IB: Actin
M
RKO cell
siNC
siNEDD4L
DSS (hr) 0 12 24 36 0 12 24 36
IB: GPX4
IB: TFRC
IB: SLC3A2
IB: NEDD4L
IB: GAPDH

Figure 6

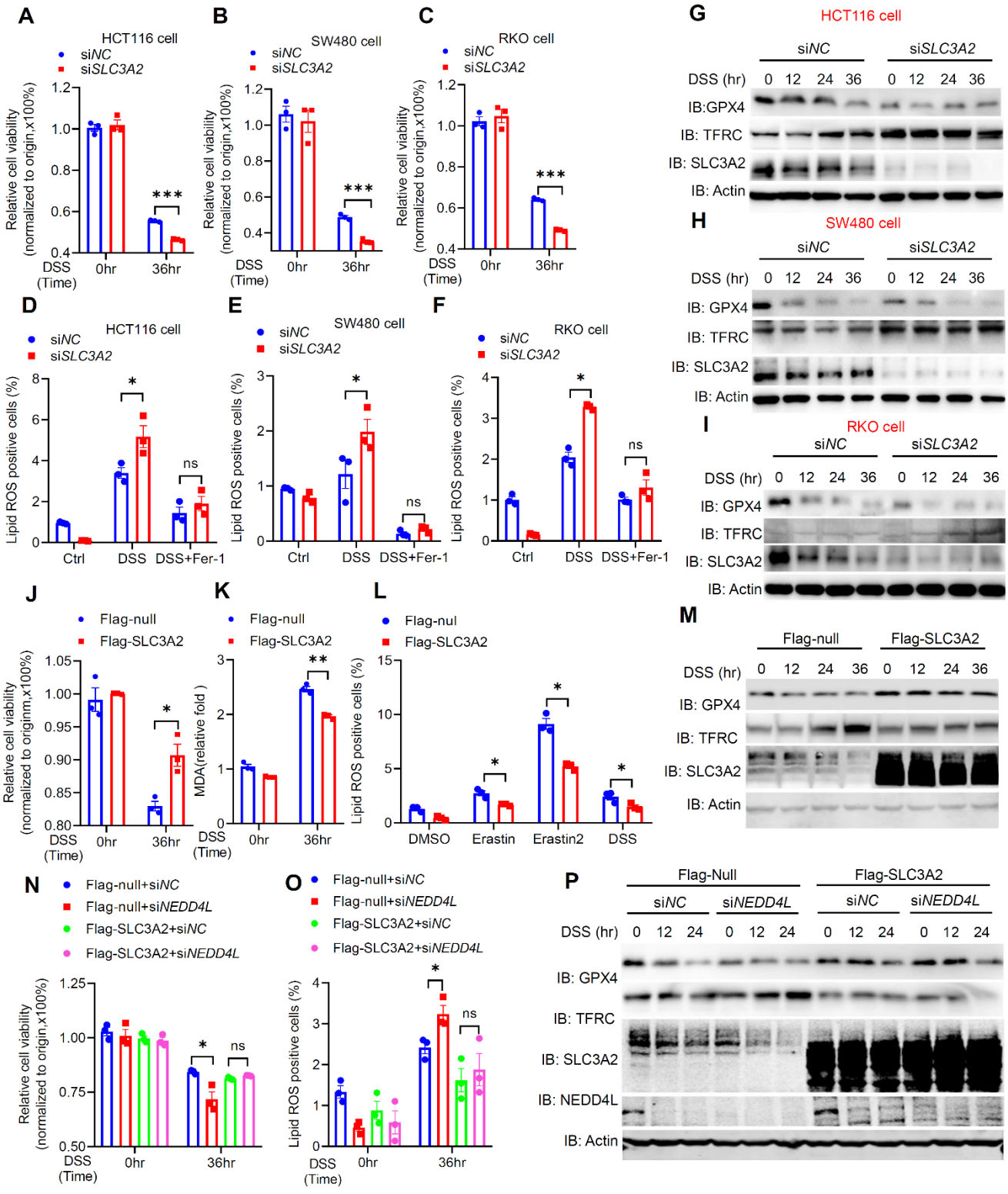
A
HCT116 cell
siNC
siSLC3A2
Relative cell viability (normalized to origin,x100%)
DSS (Time)
0hr
36hr
***
B
SW480 cell
C
RKO cell
D
Lipid ROS positive cells (%)
Ctrl
DSS
DSS+Fer-1
ns
E
F
G
HCT116 cell
siNC
siSLC3A2
DSS (hr) 0 12 24 36 0 12 24 36
IB:GPX4
IB: TFRC
IB: SLC3A2
IB: Actin
H
SW480 cell
I
RKO cell
J
Flag-null
Flag-SLC3A2
Relative cell viability (normalized to origin,x100%)
K
MDA(relative fold)
L
Lipid ROS positive cells (%)
DMSO
Erastin
Erastin2
M
N
Flag-null+siNC
Flag-null+siNEDD4L
Flag-SLC3A2+siNC
Flag-SLC3A2+siNEDD4L
O
P
Flag-Null
Flag-SLC3A2
IB: NEDD4L

Figure 7

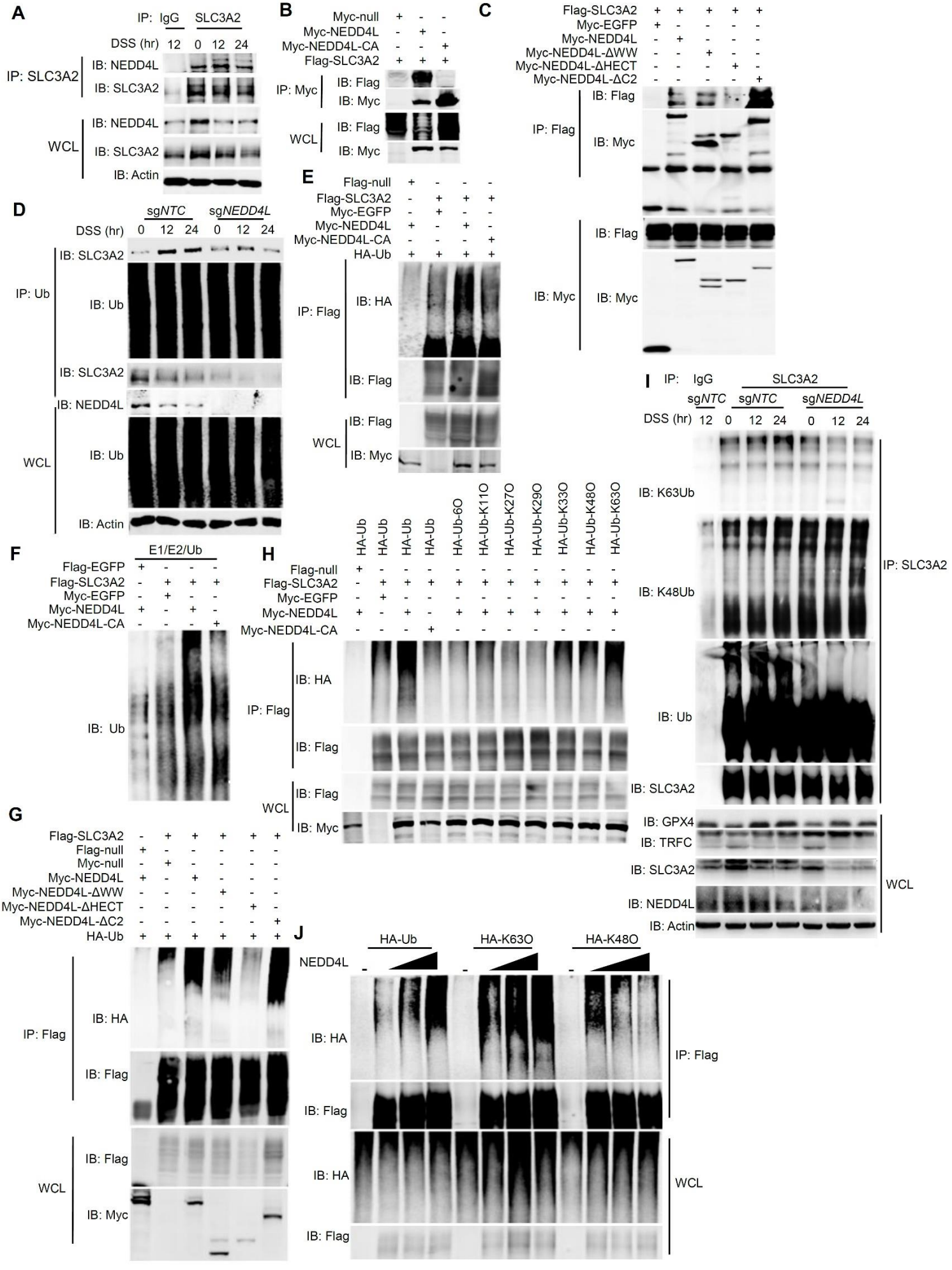
A
IP: IgG SLC3A2
DSS (hr) 12 0 12 24
IP: SLC3A2
IB: NEDD4L
IB: SLC3A2
WCL
IB: NEDD4L
IB: SLC3A2
IB: Actin
B
Myc-null + - -
Myc-NEDD4L - + -
Myc-NEDD4L-CA - - +
Flag-SLC3A2 + + +
IP: Myc
IB: Flag
IB: Myc
WCL
IB: Flag
IB: Myc
C
Flag-SLC3A2 + + + + +
Myc-EGFP + - - - -
Myc-NEDD4L - + - - -
Myc-NEDD4L-ΔWW - - + - -
Myc-NEDD4L-ΔHECT - - - + -
Myc-NEDD4L-ΔC2 - - - - +
IP: Flag
IB: Flag
IB: Myc
IB: Myc
IB: Flag
IB: Myc
D
sgNTC sgNEDD4L
DSS (hr) 0 12 24 0 12 24
IP: Ub
IB: SLC3A2
IB: Ub
IB: SLC3A2
IB: NEDD4L
WCL
IB: Ub
IB: Actin
E
Flag-null + - - -
Flag-SLC3A2 - + + +
Myc-EGFP - + - -
Myc-NEDD4L + - + -
Myc-NEDD4L-CA - - - +
HA-Ub + + + +
IP: Flag
IB: HA
IB: Flag
WCL
IB: Flag
IB: Myc
F
E1/E2/Ub
Flag-EGFP + - - -
Flag-SLC3A2 - + + +
Myc-EGFP - + - -
Myc-NEDD4L + - + -
Myc-NEDD4L-CA - - - +
IB: Ub
G
Flag-SLC3A2 - + + + + +
Flag-null + - - - - -
Myc-null - + - - - -
Myc-NEDD4L + - + - - -
Myc-NEDD4L-ΔWW - - - + - -
Myc-NEDD4L-ΔHECT - - - - + -
Myc-NEDD4L-ΔC2 - - - - - +
HA-Ub + + + + + +
IP: Flag
IB: HA
IB: Flag
WCL
IB: Flag
IB: Myc
H
HA-Ub HA-Ub HA-Ub HA-Ub HA-Ub-6O HA-Ub-K11O HA-Ub-K27O HA-Ub-K29O HA-Ub-K33O HA-Ub-K48O HA-Ub-K63O
Flag-null + - - - - - - - - - -
Flag-SLC3A2 - + + + + + + + + + +
Myc-EGFP - + - - - - - - - - -
Myc-NEDD4L + - + - + + + + + + +
Myc-NEDD4L-CA - - - + - - - - - - -
IP: Flag
IB: HA
IB: Flag
WCL
IB: Flag
IB: Myc
I
IP: IgG SLC3A2
sgNTC sgNTC sgNEDD4L
DSS (hr) 12 0 12 24 0 12 24
IB: K63Ub
IB: K48Ub
IB: Ub
IB: SLC3A2
IP: SLC3A2
IB: GPX4
IB: TRFC
IB: SLC3A2
IB: NEDD4L
IB: Actin
WCL
J
HA-Ub HA-K63O HA-K48O
NEDD4L
IB: HA
IB: Flag
IP: Flag
IB: HA
IB: Flag
WCL

Figure 8

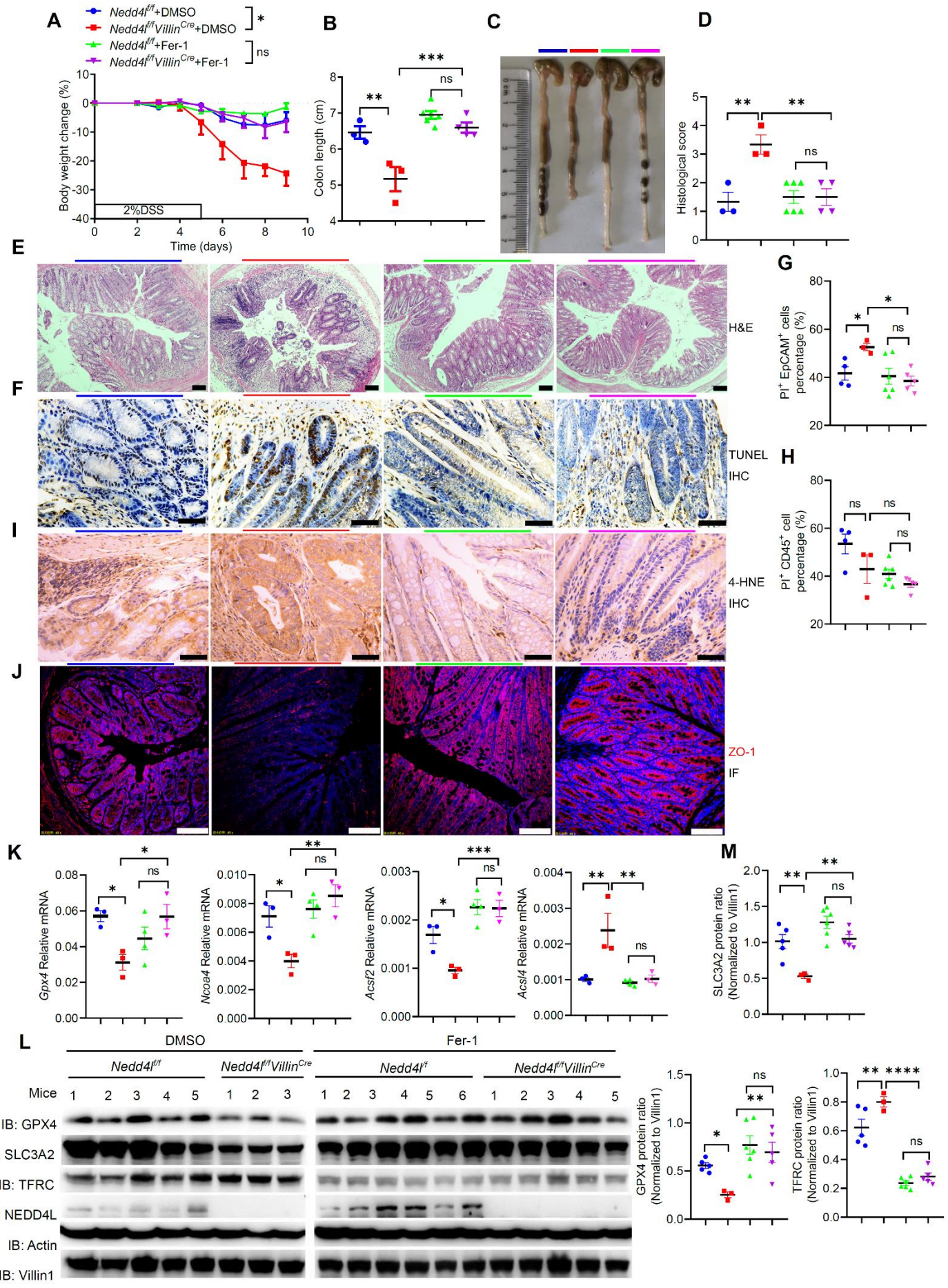
A
Nedd4l f/f+DMSO
Nedd4l f/f Villin Cre+DMSO
Nedd4l f/f+Fer-1
Nedd4l f/f Villin Cre+Fer-1
*
ns
Body weight change (%)
2%DSS
Time (days)
B
Colon length (cm)
C
D
Histological score
E
H&E
F
TUNEL
IHC
G
PI+ EpCAM+ cells percentage (%)
H
PI+ CD45+ cell percentage (%)
I
4-HNE
IHC
J
ZO-1
IF
K
Gpx4 Relative mRNA
Ncoa4 Relative mRNA
Acsf2 Relative mRNA
Acsl4 Relative mRNA
M
SLC3A2 protein ratio (Normalized to Villin1)
L
DMSO
Fer-1
Nedd4l f/f
Nedd4l f/f Villin Cre
Nedd4l f/f
Nedd4l f/f Villin Cre
Mice
IB: GPX4
IB: SLC3A2
IB: TFRC
IB: NEDD4L
IB: Actin
IB: Villin1
GPX4 protein ratio (Normalized to Villin1)
TFRC protein ratio (Normalized to Villin1)

Figure 9

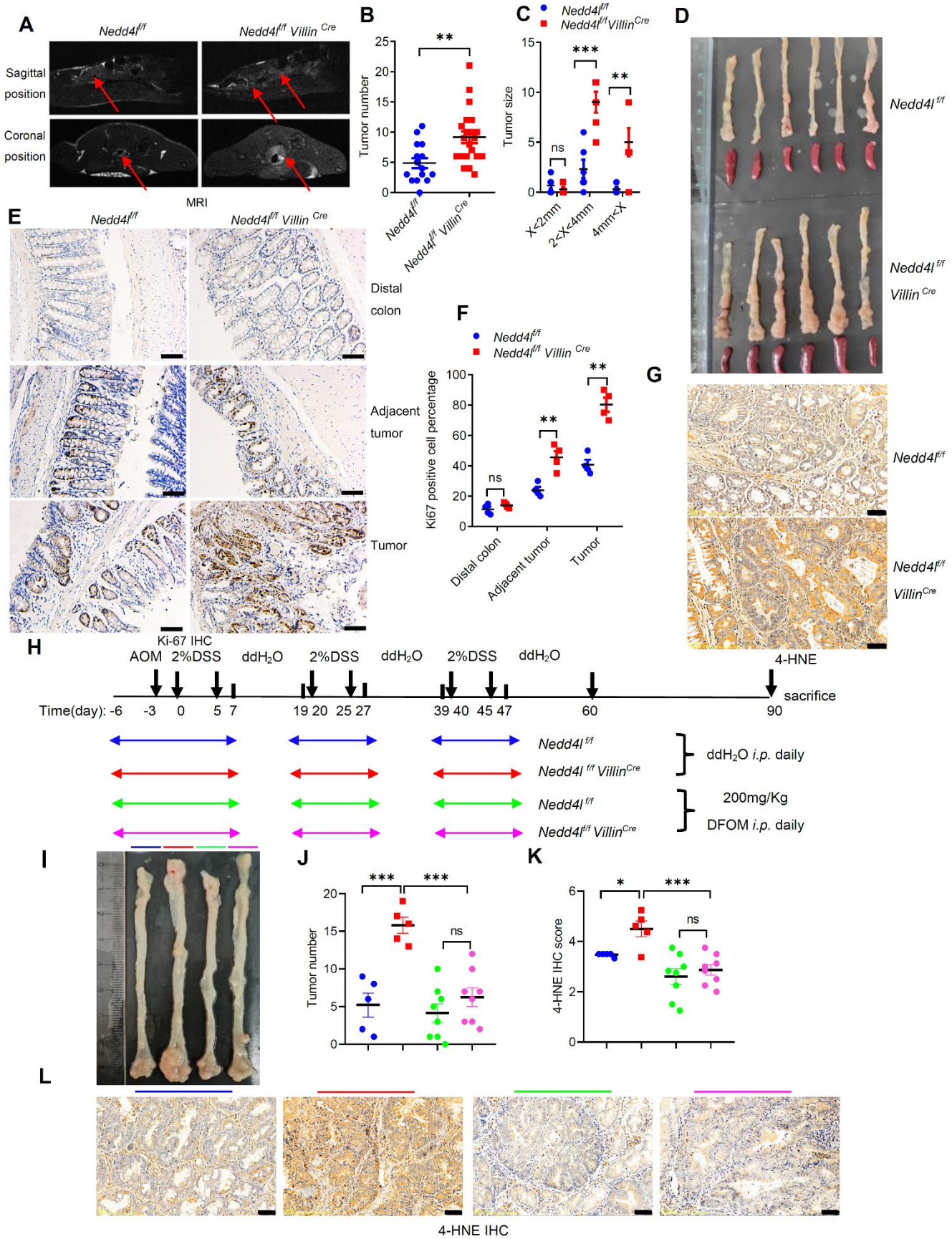
A
Nedd4l f/f
Nedd4l f/f Villin Cre
Sagittal position
Coronal position
MRI
B
Tumor number
Nedd4l f/f
Nedd4l f/f Villin Cre
C
Nedd4l f/f
Nedd4l f/f Villin Cre
Tumor size
ns
X<2mm
2<X<4mm
4mm<X
D
Nedd4l f/f
Nedd4l f/f Villin Cre
E
Nedd4l f/f
Nedd4l f/f Villin Cre
Distal colon
Adjacent tumor
Tumor
F
Nedd4l f/f
Nedd4l f/f Villin Cre
Ki67 positive cell percentage
Distal colon
Adjacent tumor
Tumor
G
Nedd4l f/f
Nedd4l f/f Villin Cre
4-HNE
H
Ki-67 IHC
AOM
2%DSS
ddH2O
2%DSS
ddH2O
2%DSS
ddH2O
Time(day): -6 -3 0 5 7 19 20 25 27 39 40 45 47 60 90
sacrifice
Nedd4l f/f
Nedd4l f/f Villin Cre
ddH2O i.p. daily
Nedd4l f/f
Nedd4l f/f Villin Cre
200mg/Kg
DFOM i.p. daily
I
J
Tumor number
K
4-HNE IHC score
L
4-HNE IHC

Figure 10

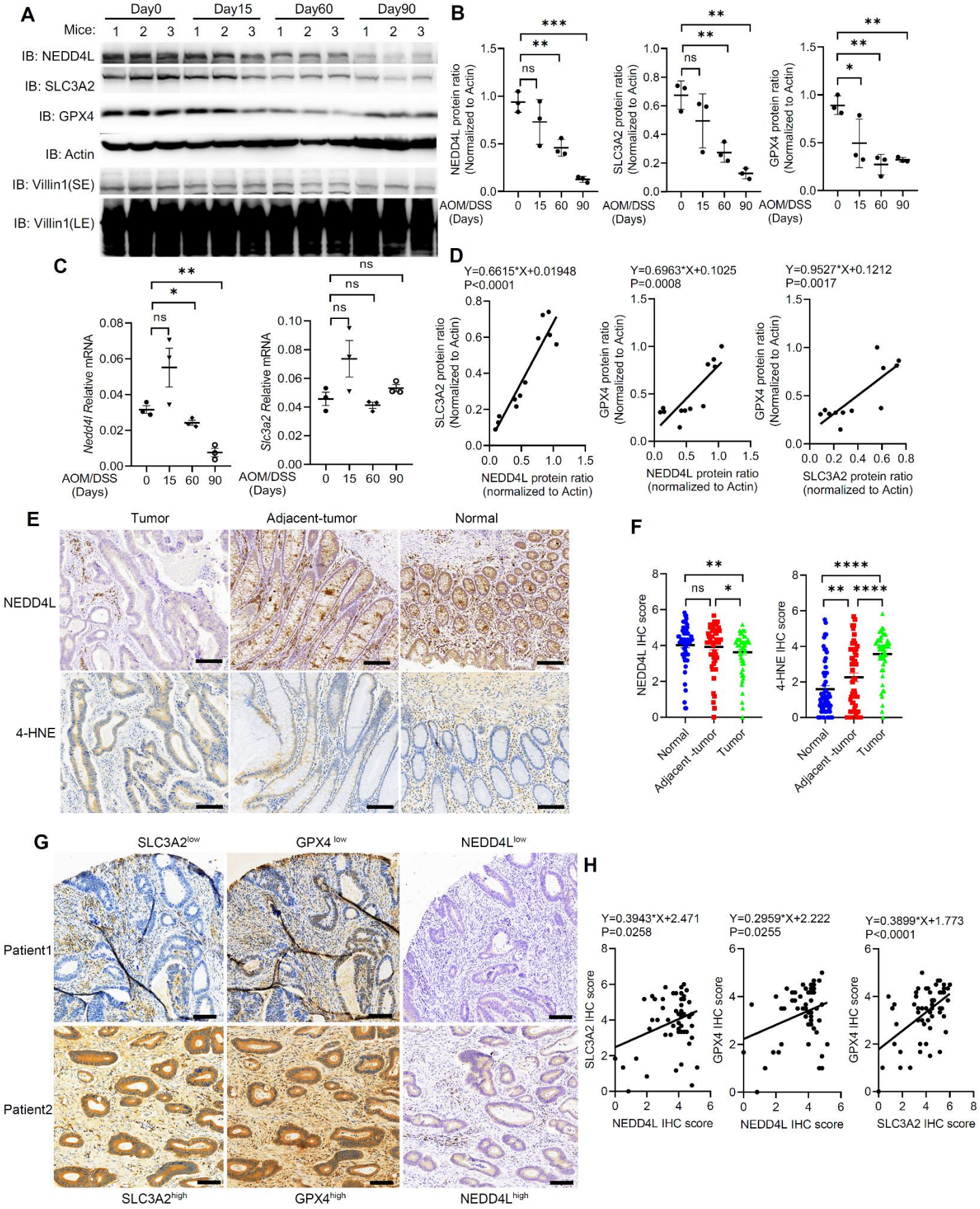
A
Day0
Day15
Day60
Day90
Mice: 1 2 3 1 2 3 1 2 3 1 2 3
IB: NEDD4L
IB: SLC3A2
IB: GPX4
IB: Actin
IB: Villin1(SE)
IB: Villin1(LE)
B
NEDD4L protein ratio (Normalized to Actin)
SLC3A2 protein ratio (Normalized to Actin)
GPX4 protein ratio (Normalized to Actin)
AOM/DSS (Days)
0 15 60 90
C
Nedd4l Relative mRNA
Slc3a2 Relative mRNA
AOM/DSS (Days)
D
Y=0.6615*X+0.01948
P<0.0001
Y=0.6963*X+0.1025
P=0.0008
Y=0.9527*X+0.1212
P=0.0017
NEDD4L protein ratio (normalized to Actin)
SLC3A2 protein ratio (normalized to Actin)
E
Tumor
Adjacent-tumor
Normal
NEDD4L
4-HNE
F
NEDD4L IHC score
4-HNE IHC score
Normal
Adjacent -tumor
Tumor
G
SLC3A2low
GPX4 low
NEDD4Llow
Patient1
Patient2
SLC3A2high
GPX4high
NEDD4Lhigh
H
Y=0.3943*X+2.471
P=0.0258
Y=0.2959*X+2.222
P=0.0255
Y=0.3899*X+1.773
P<0.0001
SLC3A2 IHC score
GPX4 IHC score
NEDD4L IHC score
SLC3A2 IHC score